Chapter 2

Channel model

2.1 Introduction

The design of communication systems, the choice of modulation and coding schemes, and the evaluation of performance require the knowledge of the end-to-end channel response in a wide range of frequencies.

In this chapter, a theoretical framework is proposed for the modeling of underground powerline access networks. A very important feature of the powerline cables is their multiconductor nature. In the light of multiconductor transmission lines theory [30], it appears that specific propagation eigenmodes may be defined for each type of cable. These correspond to specific distributions of voltages and currents that propagate with their own phase velocity and lineic attenuation, independently from each other. This aspect is generally ignored in the current publications related to measurement results [31].

A generic simulation tool was designed, that consists of several levels of abstraction :

- At the first level, Maxwell's equations are applied to the cable structure, leading to finding the distribution of the EM fields in the cable cross-section, together with charges and currents on the surface of each conductor. Conductors usually have large sections and are rather close to each other: this leads to the so-called 'proximity effect' and an heterogeneous charge distribution along each conductor surface. Considering an arbitrary cable geometry, the numerical resolution of the Laplace equation in the transverse plane provides the relevant information.

- At the second level, for a given class of metals and dielectrics, the classical primary parameters R, L, C and G are computed. Considering multi-dimensional voltages and currents, these parameters are not simple scalars but square matrices.
- At the third level, the multi-dimensional transmission line equations are solved, providing the definition and secondary parameters of the cable eigenmodes. This step implies the solution of an eigenvalue problem. With these results, a given cable segment may be modeled by a multi-dimensional scattering matrix providing transmission and reflection coefficients for each propagation mode.
- At the last level, the whole powerline access network is considered. It generally consists of a main distribution cable starting at the medium-voltage low-voltage transformer, and lying below the streets with derivation cables providing the final connection to the various subscriber buildings. Broadband modems may be connected on these termination points, just before the power meter, and transmit and/or receive digital signals to/from the central office. Cascading different cable segments, modeling the various network terminations with adequate multi-dimensional loads, and managing the derivation points finally provides the desired end-to-end channel responses.

In order to offer a better intuition on the obtained channel responses, a multipath channel model is also proposed. This model provides a very close approximation of the exact channel responses, as soon as some simplifying hypotheses are assumed. The impulse response of a cable segment, including dielectric losses and conductor losses, is firstly analyzed as a function of the segment length. The network topology is then considered, and the respective effects of derivations and terminations are analyzed to provide a multipath description of the channels. Finally, the cable losses are combined with the multipath formulation to obtain the approximated global channel responses.

2.2 Primary parameters

2.2.1 EM fields in a multiconductor structure

We consider the general case of a transmission line with N_c+1 conductors $\mathcal{C}_n$ with $n \in [0 \cdots N_c]$, where the first conductor $\mathcal{C}_0$ acts as a screen surrounding the others. The cross-section of the line is defined in the plane $(\vec{u}_x, \vec{u}_y)$

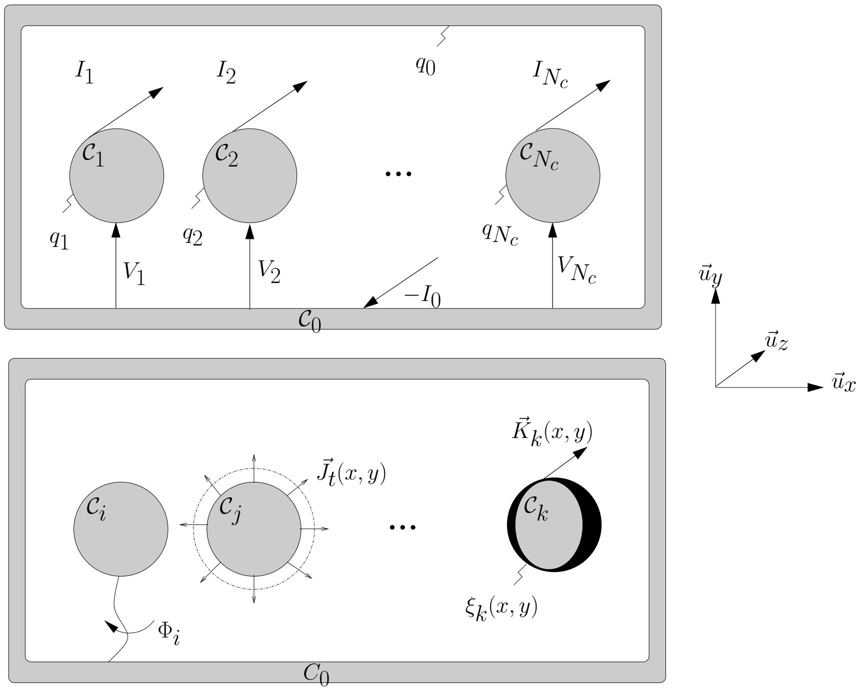

Figure 2.1: *Multiconductor structure*

whereas the longitudinal axis is aligned on $\vec{u}_z$. The dielectric medium between the conductors is supposed to be homogeneous with a dielectric constant κ. With perfect conductors, the solution of Maxwell's equations leads to the definition of TEM (Transverse Electro-Magnetic) waves propagating along $\vec{u}_z$. We define N_c *wire voltages* V_n with $n \in [1 \cdots N_c]$ with the shield conductor as the common reference, and $N_c + 1$ *wire currents* I_n with $n \in [0 \cdots N_c]$ such that $\sum_{n=1}^{N_c} I_n = -I_0$. The conductors $\mathcal{C}_n$, voltages V_n and currents I_n are illustrated in Figure 2.1.

In a so-called 'voltage-mode', voltage V_i is put to 1 while the V_j's are let to 0 with $j \neq i$. To obtain the expression of the fields in this TEM configuration, we have to solve the static EM problem corresponding to the 2-dimensional Laplace equation:

$$\nabla_t^2 \, \Phi_i(x,y) = 0 \tag{2.1}$$

with the boundary conditions:

$$\Phi_i(x,y) = \begin{cases} 1 & \text{if } (x,y) \in C_i, \ i \neq 0 \\ 0 & \text{if } (x,y) \in C_j, \ j \neq i \end{cases} \tag{2.2}$$

Once the potential function $\Phi_i(x,y)$ is known, the static transverse electric and magnetic fields $\vec{e}_t^{(i)}(x,y)$ and $\vec{h}_t^{(i)}(x,y)$ in the dielectric medium can be computed as follows:

$$\begin{aligned} \vec{e}_t^{(i)}(x,y) &= -\nabla_t\,\Phi_i(x,y) && (2.3)\\ \vec{h}_t^{(i)}(x,y) &= \frac{1}{\eta}\vec{u}_z \times \vec{e}_t^{(i)}(x,y), && (2.4)\end{aligned}$$

where $\eta = \sqrt{\mu/\varepsilon} = Z_0/\sqrt{\kappa}$ denotes the dielectric intrinsic impedance, and $Z_0 = 377\ \Omega$. The field phasors along the transmission line are given by $\vec{E}_t^{(i)}(x,y,z) = \vec{e}_t^{(i)}(x,y)\ e^{\pm\gamma z}$ and $\vec{H}_t^{(i)}(x,y,z) = \vec{h}_t^{(i)}(x,y)\ e^{\pm\gamma z}$.

The superficial charge and current densities $\xi_k^{(i)}(x,y)$ and $K_n^{(i)}(x,y)$ on the surface of the n-th conductor are then given by:

$$\begin{array}{rclcll} \xi_n^{(i)}(x,y) &=& \varepsilon|\vec{e}_t^{(i)}(x,y)| &=& -\varepsilon\frac{\partial\Phi_i(x,y)}{\partial n_n}, & (x,y)\in\mathcal{C}_n \\ K_n^{(i)}(x,y) &=& |\vec{n}_n\times\vec{h}_t^{(i)}(x,y)| &=& v\ \xi_n^{(i)}(x,y), & (x,y)\in\mathcal{C}_n \end{array} \quad (2.5)$$

where $v = 1/\sqrt{\varepsilon\,\mu} = c/\sqrt{\kappa}$ is the light velocity in the dielectric and $c = 3.10^8$ m/s. As the cross-section of the conductors is generally not small as compared with the distance between them, we have to be aware that the distribution of these charges and currents at the surface of each conductor may be largely non-uniform. The net charges $q_n^{(i)}$ and currents $I_n^{(i)}$ on a given conductor are obtained by integration on the contour $\mathcal{C}_n$:

$$q_n^{(i)} = \oint_{\mathcal{C}_n} \xi_n^{(i)}(x,y)\,dl \qquad\qquad I_n^{(i)} = \oint_{\mathcal{C}_n} K_n^{(i)}(x,y)\,dl \qquad (2.6)$$

Finally, the magnetic flux $\phi_n^{(i)}$ through an arbitrary line joining $\mathcal{C}_0$ and $\mathcal{C}_n$ is:

$$\begin{aligned} \phi_n^{(i)} &= \int_{(x_0,y_0)\in\mathcal{C}_0}^{(x_n,y_n)\in\mathcal{C}_n} \vec{n}\ .\ \mu\vec{h}_t^{(i)}(x,y)\,dl && (2.7)\\ &= \frac{\mu}{\eta}\left[\Phi_i(x_n,y_n) - \Phi_i(x_0,y_0)\right] = \frac{1}{v}\,\delta_{in} && (2.8)\end{aligned}$$

Figure 2.1 illustrates the superficial charge and current densities defined in (2.5), as well as the magnetic flux given by (2.8).

The different quantities $x^{(i)}$ defined above are valid for a given voltage mode i. More generally, the voltage distribution on the conductors will be arbitrary and given by the column vector $\underline{V}$. By the superposition principle, the corresponding quantities will be given by $x = \sum_{i=1}^{N} V_i \, x^{(i)}$.

The solution of the static EM problem (2.1)-(2.2) can be obtained numerically for an arbitrary configuration of the line cross-section. The computation of the charge density profile $\xi_n^{(i)}(x,y)$ on each conductor contour $\mathcal{C}_n$ and for each voltage mode i is actually sufficient to derive the primary parameters of the multiconductor transmission line. In the method proposed by [32], each conductor contour is approximated by a polygon with a large number of sides carrying a uniform charge density, and the densities on each side have to be found in order to recover the original boundary conditions given by (2.2). Figure 2.2 displays the charge density profiles $\xi_n(x,y)$ obtained with this method, for three types of voltage configurations. The multiconductor structure considered here includes 4 circular inner conductors and 1 circular screen. The bold lines give the conductor contours. The numbers inside each inner conductor give the wire voltage V_n (in volts) with respect to the external conductor. The line segments normal to the conductor contours give the local charge (and current) densities. Segments outside the conductors correspond to positive charges while segments inside the conductors correspond to negative charges. The three voltage configurations used here actually correspond to the *eigenmodes* of the multiconductor cable, as will be explained in Section 2.3.

2.2.2 Capacitance and external inductance

The capacitance matrix $\underline{\underline{C}}_w$ gives the global relation between the net charges q_n on the N_c inner conductors and the wire voltages V_n :

$$\begin{bmatrix} q_1 \\ \vdots \\ q_{N_c} \end{bmatrix} = \left[\underline{\underline{C}}_w\right] \begin{bmatrix} V_1 \\ \vdots \\ V_{N_c} \end{bmatrix} \tag{2.9}$$

From the definition of the voltage modes, it clearly appears that:

$$\left(\underline{\underline{C}}_w\right)_{n,i} = q_n^{(i)} = -\varepsilon \oint_{\mathcal{C}_n} \frac{\partial \Phi_i(x,y)}{\partial n_n} \tag{2.10}$$

From the relations above, it can easily be shown that the voltages and currents are related by :

$$v \, \underline{\underline{C}}_w \, \underline{V} = \underline{I} \tag{2.11}$$

for any progressive wave (i.e. with a propagation factor $e^{-\gamma z}$).

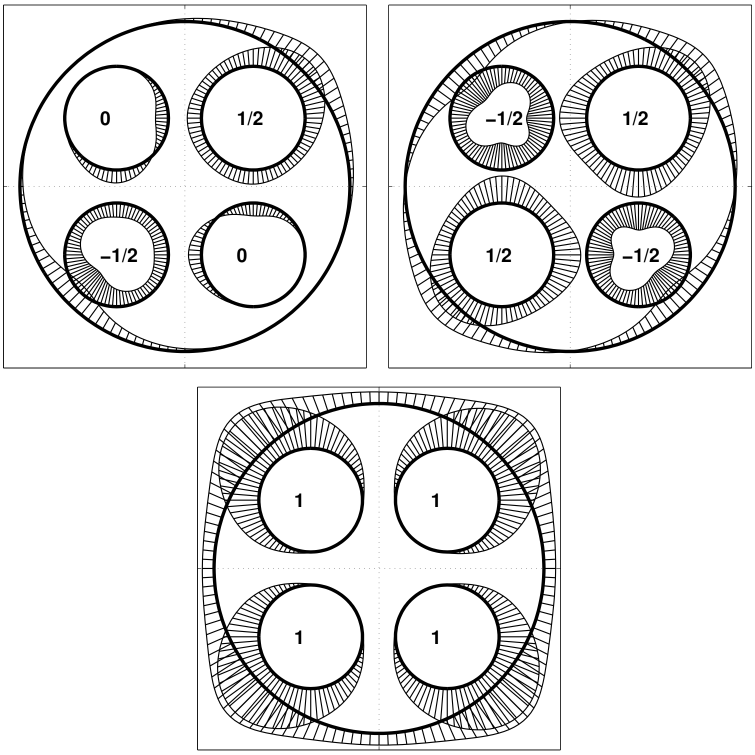

Figure 2.2: *Distribution of local currents for a unit line voltage in the different propagation modes : differential (up), phantom (middle) and common mode (down)*

The external inductance matrix $\underline{\underline{\mathrm{L}}}_w$ gives the global relation between the magnetic fluxes ϕ_n and the wire currents I_n :

$$\begin{bmatrix} \Phi_1 \\ \vdots \\ \Phi_{N_c} \end{bmatrix} = \left[\underline{\underline{\mathrm{L}}}_w\right] \begin{bmatrix} I_1 \\ \vdots \\ I_{N_c} \end{bmatrix} \tag{2.12}$$

From (2.8), it appears that $\underline{\phi} = 1/v\,\underline{\mathrm{V}}$. By (2.11), this implies the next relation between the capacitance and inductance matrices:

$$\underline{\underline{\mathrm{L}}}_w\,\underline{\underline{\mathrm{C}}}_w = \frac{1}{v^2}\underline{\underline{\mathrm{E}}}_{N_c} = \underline{\underline{\mathrm{C}}}_w\,\underline{\underline{\mathrm{L}}}_w \tag{2.13}$$

where $\underline{\underline{\mathrm{E}}}_{N_c}$ is the identity matrix of size N_c. The counterpart of equation

(2.11) is :

$$v \underline{\underline{\mathrm{L}}}_w \underline{\mathrm{I}} = \underline{\mathrm{V}} \tag{2.14}$$

for any progressive wave.

2.2.3 Dielectric losses

Non perfect dielectrics are characterized by a complex permittivity $\varepsilon = \varepsilon' - j\,\varepsilon''$. The imaginary part ε'' encompasses both conduction and polarization losses. A transverse conduction current flowing between the conductors dissipates a part of the wave power. The conduction current density in the medium is given by $\vec{J}_t(x,y) = \omega\,\varepsilon''\,\vec{e}_t(x,y)$. Integrating around each inner conductor, we obtain the net transverse current per unit length :

$$I_{tn} = \oint_{\mathcal{C}_n} \vec{J}_t(x,y).\vec{n}\,dl = \omega\,\varepsilon''\frac{1}{\varepsilon'}\,q_n = \delta_d\,\omega\,q_n \tag{2.15}$$

where the dielectric loss angle δ_d is defined as $\mathrm{tg}(\delta_d) \approx \delta_d = \varepsilon''/\varepsilon'$. Figure 2.1 illustrates the conduction current density around conductor $\mathcal{C}_j$.

The conductance matrix $\underline{\underline{\mathrm{G}}}_w$ gives the relation between the transverse conduction currents I_{tn} and the wire voltages V_n :

$$\begin{bmatrix} I_{t1} \\ \vdots \\ I_{tN_c} \end{bmatrix} = \left[\underline{\underline{\mathrm{G}}}_w\right] \begin{bmatrix} V_1 \\ \vdots \\ V_{N_c} \end{bmatrix} \tag{2.16}$$

Inserting (2.15) into (2.9), it follows that the conductance matrix is given by :

$$\underline{\underline{\mathrm{G}}}_w = \delta_d\,\omega\,\underline{\underline{\mathrm{C}}}_w. \tag{2.17}$$

2.2.4 Conductor losses

In this section, we take into account the skin effect caused by the finite conductivity of the conductors. Non perfect conductors have a finite conductivity σ_n with $n \in (0 \cdots N_c)$. It follows that a longitudinal electric field appears at the surface of the conductors:

$$\vec{e}^{(i)}_{z,n}(x,y) = \eta_n\,K^{(i)}_n(x,y) \qquad (x,y) \in \mathcal{C}_n \tag{2.18}$$

with η_n the metal surface impedance:

$$\eta_n = \sqrt{\frac{j\,\omega\,\mu_n}{\sigma_n}} = (1+j)\,R_{mn} = \frac{(1+j)}{\sigma_n\,\delta_n}. \tag{2.19}$$

$\delta_n = \sqrt{\frac{1}{2\omega\mu_n\sigma_n}}$ and $R_{mn} = \sqrt{\frac{\omega\,\mu_n}{2\,\sigma_n}}$ are the skin depth and surface resistance associated with the n-th conductor.

In a small perturbation approach, we assume that the transverse fields and related quantities are unaffected by the skin effect. On the other hand, longitudinal fields must be re-computed as they change from zero to a finite value.

To define the resistance matrix $\underline{\underline{\mathrm{R}}}_w$, the direct use of the longitudinal voltage drop induced along the line by the current flow is not a valid approach as this voltage drop is not uniquely defined. Indeed, the longitudinal fields $\vec{e}_{z,n}(x,y)$ and current densities $K_n(x,y)$ are largely non-uniform on each conductor contour. To keep a classical transmission line formalism, we introduce a kind of 'mean longitudinal voltage drop' per unit length $\underline{\mathrm{U}}$ such that:

$$\underline{\mathrm{U}} = \underline{\underline{\mathrm{R}}}_{wc}\,\underline{\mathrm{I}} \tag{2.20}$$

where $\underline{\underline{\mathrm{R}}}_{wc}$ is a complex matrix. The complex power dissipated in the conductors per unit length is given by:

$$P_c = \frac{1}{2}\underline{\mathrm{I}}^*\underline{\mathrm{U}} = \frac{1}{2}\left[\begin{array}{ccc} I_1^* & \cdots & I_{N_c}^* \end{array}\right]\left[\underline{\underline{\mathrm{R}}}_{wc}\right]\left[\begin{array}{c} I_1 \\ \vdots \\ I_{N_c} \end{array}\right] \tag{2.21}$$

To obtain a valid expression of the resistance matrix, the last quantity has to be the same as the complex power corresponding to the transverse component of the Poynting vector $\vec{S}(x,y)$. This can be computed as:

$$\begin{aligned} -\vec{n}_n\,.\,\vec{S}(x,y) &= \frac{1}{2}\vec{e}_l(x,y)\times\vec{h}_t^*(x,y) && (2.22)\\ &= \frac{1}{2}\eta_n|K_n(x,y)|^2 = \frac{v^2\,\eta_n}{2}|\xi_n(x,y)|^2 && (2.23) \end{aligned}$$

The corresponding complex power is obtained by integrating on each contour and summing the contributions of the N_c+1 conductors:

$$P_c = \frac{v^2}{2}\sum_{n=0}^{N_c}\eta_n\oint_{\mathcal{C}_n}|\xi_n(x,y)|^2\,dl \tag{2.24}$$

This quantity must be calculated for an arbitrary voltage configuration $\underline{\mathrm{V}}$. Let us introduce a matrix $\underline{\underline{\mathrm{A}}}$ whose entry (i,j) is defined as:

$$\left(\underline{\underline{\mathrm{A}}}\right)_{i,j} = v^4\sum_{n=0}^{N_c}\eta_n\oint_{\mathcal{C}_n}\xi_n^{(i)}(x,y)\,\xi_n^{(j)}(x,y)\,dl \tag{2.25}$$

The complex power is now:

$$P_c = \frac{1}{2v^2}\,\underline{V}^*\underline{\underline{A}}\,\underline{V} = \frac{1}{2}\,\underline{I}^*\left[\underline{\underline{L}}_w^*\underline{\underline{A}}\,\underline{\underline{L}}_w\right]\underline{I} \tag{2.26}$$

where relation (2.14) was used. Comparing expressions (2.21) and (2.26), we finally obtain the resistance matrix as:

$$\underline{\underline{R}}_{wc} = \underline{\underline{L}}_w^*\underline{\underline{A}}\,\underline{\underline{L}}_w. \tag{2.27}$$

From the expression of η_n, it appears that this matrix is complex with the imaginary part equal to the real part. This matrix indeed encompasses both the resistance matrix $\underline{\underline{R}}_w$ corresponding to conductor losses and the internal inductance matrix which has to be added to the external inductance matrix $\underline{\underline{L}}_w$ previously calculated:

$$\underline{\underline{R}}_{wc} = (1+j)\,\underline{\underline{R}}_w \tag{2.28}$$

It should be observed that each of the $N_c + 1$ conductors plays a role in the computation of the lineic resistance matrix. Whatever the voltage configuration, local currents are induced along the contour of each conductor, which implies power dissipation, even if the mean current integrated along the corresponding contour is zero. Consider for instance the distribution of local currents given by the first scheme in Figure 2.2. The net currents I_n are zero for conductors $\mathcal{C}_1$ and $\mathcal{C}_3$ (with wire voltages equal to 0), and for the external conductor $\mathcal{C}_0$. Local currents are generated, however, in these three conductors, which contributes to power dissipation.

2.3 Secondary parameters

2.3.1 Multiconductor line equations

Transmission line equations may be written in matrix form:

$$\frac{d\underline{I}}{dz} = -\left[\underline{\underline{y}}\right]\,\underline{V} \qquad\qquad \frac{d\underline{V}}{dz} = -\left[\underline{\underline{z}}\right]\,\underline{I} \tag{2.29}$$

where $\underline{\underline{y}}$ and $\underline{\underline{z}}$ are lineic admittance and impedance matrices. The solution to these equations is given in [33]. After derivation and elimination, these equations transform into:

$$\frac{d^2\underline{I}}{dz^2} = \left[\underline{\underline{y}}\,\underline{\underline{z}}\right]\underline{I} \qquad\qquad \frac{d^2\underline{V}}{dz^2} = \left[\underline{\underline{z}}\,\underline{\underline{y}}\right]\,\underline{V} \tag{2.30}$$

As results from electromagnetic reciprocity, $\underline{\underline{y}}$ and $\underline{\underline{z}}$ are symmetric matrices, and $\underline{\underline{y}}\,\underline{\underline{z}}$ and $\underline{\underline{z}}\,\underline{\underline{y}}$ are the transposed of each other. As a consequence, they have the same eigenvalues. Let γ_m^2, with $m \in \{1, \cdots, M\}$ be the M distinct eigenvalues of $\underline{\underline{y}}\,\underline{\underline{z}}$ and $\underline{\underline{z}}\,\underline{\underline{y}}$, with $M \leq N_c$. Each eigenvalue γ_m^2 has an algebraic multiplicity $\pi(m)$ with $\sum_m \pi(m) = N_c$. Multiple eigenvalues generally appear when the considered transmission line presents some kind of symmetry, which is the case for many powerline cables.

Equations (2.30) have a set of N_c linearly independent solutions, the *eigenmodes*, of the form:

$$\underline{I}(z) = \underline{I}_n \exp(\pm\gamma_n z) \qquad\qquad \underline{V}(z) = \underline{V}_n \exp(\pm\gamma_n z) \tag{2.31}$$

where $\underline{I}_n$, $\underline{V}_n$ and γ_n are solutions of the eigenvalue problems:

$$\left[\underline{\underline{y}}\,\underline{\underline{z}}\right] \underline{I}_n = \gamma_n^2 \underline{I}_n \qquad\qquad \left[\underline{\underline{z}}\,\underline{\underline{y}}\right] \underline{V}_n = \gamma_n^2 \underline{V}_n \tag{2.32}$$

Building a diagonal matrix $\underline{\underline{\Gamma}} = \text{Diag}\left[\gamma_n^2\right]$ with the N_c eigenvalues and two modal matrices $\underline{\underline{J}}$ and $\underline{\underline{U}}$, the columns of which are the eigenvectors $\underline{I}_n$ and $\underline{V}_n$, respectively, the eigenvalue problems may be written:

$$\left[\underline{\underline{y}}\,\underline{\underline{z}}\right] \underline{\underline{J}} = \underline{\underline{J}}\,\underline{\underline{\Gamma}} \qquad\qquad \left[\underline{\underline{z}}\,\underline{\underline{y}}\right] \underline{\underline{U}} = \underline{\underline{U}}\,\underline{\underline{\Gamma}} \tag{2.33}$$

2.3.2 Normalization

The modal matrices $\underline{\underline{U}}$ and $\underline{\underline{J}}$ may not be chosen independently. Actually, using (2.29) and (2.31), they are linked by the following constraint :

$$\underline{\underline{J}}\,\underline{\underline{\Gamma}}\,\underline{\underline{U}}^{-1} = \underline{\underline{y}} \qquad\qquad \underline{\underline{U}}\,\underline{\underline{\Gamma}}\,\underline{\underline{J}}^{-1} = \underline{\underline{z}} \tag{2.34}$$

On the other hand, the eigenvectors $\underline{I}_n$ or $\underline{V}_n$ are not fully defined by the eigenvalues problems (2.33) : each eigenvector can be individually scaled, and the definition of a given basis in the subspace corresponding to a multiple eigenvalue is arbitrary. Additional constraints are necessary to make the solution unique.

Using (2.33) and (2.34), it can be shown that :

$$\underline{\underline{U}}^T \left(\underline{\underline{y}}\right) \underline{\underline{U}} = \left(\underline{\underline{U}}^T \underline{\underline{J}}\right) \underline{\underline{\Gamma}} = \underline{\underline{\Gamma}} \left(\underline{\underline{U}}^T \underline{\underline{J}}\right) = \underline{\underline{J}}^T \left(\underline{\underline{z}}\right) \underline{\underline{J}} \tag{2.35}$$

As $\underline{\underline{\Gamma}}$ is diagonal, (2.35) implies that the matrix product $\underline{\underline{U}}^T \underline{\underline{J}}$ is block-diagonal :

$$\underline{\underline{U}}^T \underline{\underline{J}} = \text{Diag}\left[\underline{\underline{X}}_m\right] \tag{2.36}$$

where each block $\underline{\underline{X}}_m$ is a symmetric matrix of size $\pi(m)$. From matrix theory, it is known (cf. [34], pp. 207) that for any symmetric matrix $\underline{\underline{X}}_m$, there exists a matrix $\underline{\underline{Y}}_m$ such that $\underline{\underline{X}}_m = \underline{\underline{Y}}_m^T \underline{\underline{Y}}_m$. We define the normalized modal matrices as follows :

$$\underline{\underline{U}}_0 = \underline{\underline{U}} \,\mathrm{Diag}\left[\underline{\underline{Y}}_m^{-1}\right] \qquad \underline{\underline{J}}_0 = \underline{\underline{J}} \,\mathrm{Diag}\left[\underline{\underline{Y}}_m^{-1}\right] \tag{2.37}$$

The normalized eigenvectors $\underline{I}_{0n}$ and $\underline{V}_{0n}$ are mutually orthonormal :

$$\underline{\underline{U}}_0^T \underline{\underline{J}}_0 = \underline{\underline{E}}_N \tag{2.38}$$

Another form of this normalization condition is given by :

$$\underline{\underline{U}}_0^T \,\underline{\underline{y}}\, \underline{\underline{U}}_0 = \underline{\underline{\Gamma}} = \underline{\underline{J}}_0^T \,\underline{\underline{z}}\, \underline{\underline{J}}_0 \tag{2.39}$$

2.3.3 Progressive and regressive waves

The general solution of the multiconductor line equations is finally given by :

$$\underline{V}(z) = \underline{\underline{U}}_0 \left[\underline{A}(z) + \underline{B}(z)\right] \qquad \underline{I}(z) = \underline{\underline{J}}_0 \left[\underline{A}(z) - \underline{B}(z)\right] \tag{2.40}$$

with

$$\underline{A}(z) = \mathrm{Diag}\left[\exp\left(-\gamma_n z\right)\right] \underline{A} \qquad \underline{B}(z) = \mathrm{Diag}\left[\exp\left(+\gamma_n z\right)\right] \underline{B} \tag{2.41}$$

where $\underline{A}$ and $\underline{B}$ are two column vectors of arbitrary constants to be determined by the boundary conditions. This very compact form of the solutions shows progressive and regressive eigenmodes with amplitudes $\underline{A}$ and $\underline{B}$.

Let us assume for instance that the boundary conditions are such that $A_n \neq 0$, all other elements of $\underline{A}$ and all elements of $\underline{B}$ being zero. Then the voltages and currents are given by

$$\underline{V}\,(z) = A_n \,\underline{V}_{0n}\, e^{-\gamma_n z} \qquad \underline{I}\,(z) = A_n \,\underline{I}_{0n}\, e^{-\gamma_n z}. \tag{2.42}$$

The normalized eigenvectors $\underline{I}_{0n}$ and $\underline{V}_{0n}$ give the distributions of voltages and currents for the n-th eigenmode and A_n is an amplitude factor. A given eigenmode is thus characterized by well defined distributions of voltages and currents, with a common propagation factor $e^{-\gamma_n z}$ for these voltages and currents. Thanks to the normalization condition (2.38), the scalars $A_n^2/2$ and $B_n^2/2$ give the complex power carried by the progressive and regressive waves, respectively, by the n-th eigenmode.

The concepts of characteristic impedance Z_c and admittance Y_c may be extended to the multidimensional case. Defining $(\underline{V}_+(z), \underline{I}_+(z))$ as the progressive waves, we get :

$$\begin{array}{rcccl} \underline{V}_+(z) & = & \left(\underline{\underline{UU^T}}\right)\underline{I}_+(z) & = & \underline{\underline{Z}}_C\underline{I}_+(z) \\ \underline{I}_+(z) & = & \left(\underline{\underline{JJ^T}}\right)\underline{V}_+(z) & = & \underline{\underline{Y}}_C\underline{V}_+(z) \end{array} \tag{2.43}$$

2.3.4 Line voltages

In Section 2.2.1, voltages were arbitrarily defined as the wire voltages with respect to the external screen, considered as a common reference. Currents were defined as the internal wire currents, whose sum gave rise to an equivalent current flowing in the opposite direction inside the external screen. These definitions correspond to a 'wire' formulation. Actually, there are alternative ways of defining voltages and currents in a multiconductor structure. A 'line' formulation may be more useful to describe the cable behavior. For instance, for a two-wire transmission line under a screen, one may prefer the use of the differential mode and common mode voltages and currents, rather than the individual wire voltages and currents.

The changes of variables between the 'wire' and the 'line' formulations is constrained to linear transformations of the type :

$$\underline{V}_L = \underline{\underline{N}}^{-1}\underline{V}_w \qquad\qquad \underline{I}_L = \underline{\underline{N}}^T\underline{I}_w \tag{2.44}$$

so as to maintain the power as given by $P = \frac{1}{2}I_L^*V_L = \frac{1}{2}I_w^*V_w$. It follows from (2.29) and (2.44) that the pair $(\underline{V}_L, \underline{I}_L)$ also obeys transmission lines equations. The corresponding change of variables for the lineic parameters is given by:

$$\underline{\underline{z}}_L = \underline{\underline{N}}^{-1}\underline{\underline{z}}_w\left(\underline{\underline{N}}^T\right)^{-1} \qquad\qquad \underline{\underline{y}}_L = \underline{\underline{N}}^T\underline{\underline{y}}_w\underline{\underline{N}} \tag{2.45}$$

There is an infinite number of ways to define a 'line' formulation, as this amounts to selecting an arbitrary matrix $\underline{\underline{N}}$. A pertinent choice leads to the diagonalization of the previously defined matrices. Let us select the columns of $\underline{\underline{N}}$ as a set of eigenvectors $\underline{V}_{0w}$:

$$\underline{\underline{N}} = \left[\begin{array}{ccc} V_{0w}^{(1)} & \cdots & V_{0w}^{(N_c)} \end{array}\right] \tag{2.46}$$

The amplitude of each eigenvector is here chosen to get a tractable expression of the resulting line voltages. Furthermore, as shown in last section, the eigenvectors corresponding to a multiple eigenvalue have to be chosen adequately. The resulting modal matrices $\underline{\underline{\mathrm{U}}}_{0L} = \underline{\underline{\mathrm{N}}}^{-1}\,\underline{\underline{\mathrm{U}}}_{0w}$ and $\underline{\underline{\mathrm{J}}}_{0L} = \underline{\underline{\mathrm{N}}}^{T}\,\underline{\underline{\mathrm{J}}}_{0w}$ are diagonal. This means that each line voltage and current propagates along the cable with its own propagation factor γ_n. From (2.39) and (2.43), it follows that the corresponding matrices $\underline{\underline{\mathrm{y}}}_L$, $\underline{\underline{\mathrm{z}}}_L$, $\underline{\underline{\mathrm{Z}}}_{CL}$ and $\underline{\underline{\mathrm{Y}}}_{CL}$ are also diagonal. In particular:

$$\underline{\underline{\mathrm{U}}}_{0L} = \mathrm{Diag}\left(\sqrt{Z_{C_n}}\right) \qquad \underline{\underline{\mathrm{J}}}_{0L} = \mathrm{Diag}\left(\sqrt{Y_{C_n}}\right) \tag{2.47}$$

with $Z_{C_n} = 1/Y_{C_n}$.

2.3.5 Application to powerline cables

In this section, the general results obtained in Sections 2.2 and 2.3 are applied to the case of low-voltage powerline cables used in the underground power distribution network. Figure 2.3 illustrates the cross-section of typical PLC cables with 3 or 4 inner conductors. The external conductor $\mathcal{C}_0$ is a circle of radius b. The internal conductors $\mathcal{C}_n$ are constrained inside a circle of radius a, and are surrounded by a dielectric sheath with a thickness $\Delta = b - a$.

Section 2.2 gives the expression of the lineic impedance and admittance matrices in the 'wire' formulation :

$$\begin{aligned} \underline{\underline{\mathrm{z}}}_w(f) &= (1+j)\,\underline{\underline{\mathrm{R}}}_w(f) + \frac{j\omega}{v^2}\,\underline{\underline{\mathrm{C}}}_w^{-1} && (2.48) \\ \underline{\underline{\mathrm{y}}}_w(f) &= (j+\delta_d)\,\omega\,\underline{\underline{\mathrm{C}}}_w && (2.49) \end{aligned}$$

where the lineic capacitance and resistance matrices are given by

$$\underline{\underline{\mathrm{C}}}_w = \varepsilon \begin{bmatrix} c_{11} & c_{12} & \cdots & c_{1N} \\ c_{12} & c_{22} & & \vdots \\ \vdots & & \ddots & \\ c_{1N} & \cdots & & c_{NN} \end{bmatrix} \tag{2.50}$$

$$\underline{\underline{\mathrm{R}}}_w = \sum_{k=0}^{N_c} \frac{R_{mk}(f)}{b} \begin{bmatrix} r_{11} & r_{12} & \cdots & r_{1N} \\ r_{12} & r_{22} & & \vdots \\ \vdots & & \ddots & \\ r_{1N} & \cdots & & r_{NN} \end{bmatrix}_k \tag{2.51}$$

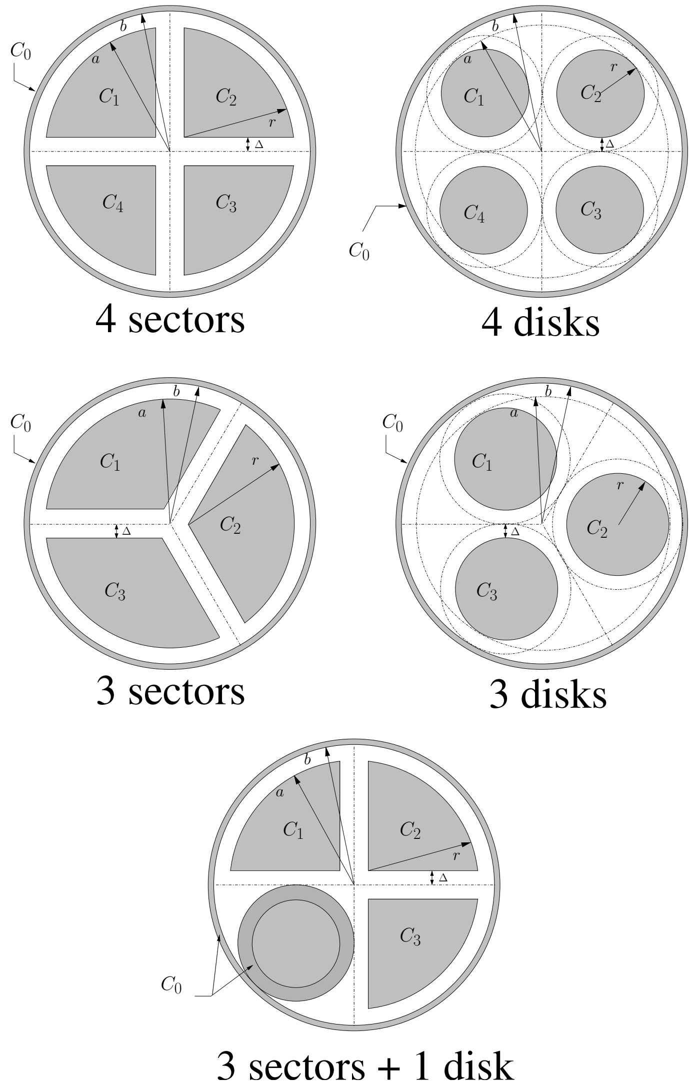

Figure 2.3: *Cross-section of 4-conductor and 3-conductor symmetric cables*

The computation of the adimensional entries c_{ij} and r_{ij} in the last expressions requires the resolution of the Laplace equation in the cable cross-section. For example, with the classical coax cable ($N_c = 1$) with dimensions a and b, the solution is given by [35]

$$c_{11} = \frac{2\pi}{\log(b/a)} \qquad\qquad r_{11} = \frac{1}{2\pi}\left(1 + \frac{b}{a}\right) \tag{2.52}$$

For a fixed cable structure (as given by one of the schemes in Figure 2.3), the parameters c_{ij} and r_{ij} only depend on the ratio $\rho = \frac{a}{b}$. The cable size b has no effect on the capacitance matrix, while the entries of the resistance matrix decrease as $1/b$ as suggested by equation (2.51). Taking into account the symmetry of matrices $\underline{\underline{\mathrm{C}}}_w$ and $\underline{\underline{\mathrm{R}}}_w$, i.e. $c_{ij} = c_{ji}$ and $r_{ij} = r_{ji}$, the solution of this geometrical problem finally provides $N_c^2 + N_c$ distinct real coefficients $\{c_{ij}\}$ and $\{r_{ij}\}$.

As explained in Section 2.3.4, the multiconductor transmission line analysis can also be performed in a 'line' formulation corresponding to the cable eigenmodes. The associated resistance and capacitance matrices are known to be diagonal. The diagonal entries can be written :

$$C_n = \varepsilon\, c_n(\rho) \qquad R_n = \sum_{k=0}^{N} \frac{R_{mk}(f)}{b} r_{nk}(\rho) = \frac{R_m(f)}{b}\, r_n(\rho) \tag{2.53}$$

where the last equality is only valid if all conductors have the same surface resistance R_m. The corresponding lineic inductances and admittances are

$$L_n = \frac{\mu}{c_n(\rho)} \qquad\qquad G_n = (2\pi f)\ \delta_d\, \varepsilon\, c_n(\rho) \tag{2.54}$$

In addition to the $2N_c$ geometrical parameters c_n and r_n, $N_c^2 - N_c$ parameters are actually needed to express the line voltages as a function of the wire voltages, according to equation (2.46), and considering that each eigenvector can be arbitrarily scaled. Both line and wire formulations of the solution thus require the same amount of $N_c^2 + N_c$ real parameters. As soon as there is some kind of geometrical symmetry in the cross-section, the number of relevant parameters generally decreases (examples will be given in Section 2.3.6).

Secondary parameters provide a meaningful description of the cable behavior. They are the lineic attenuation $\alpha_n(f)$, the phase velocity $v_n(f)$ and the complex characteristic impedance $Z_{C_n}(f)$ for each eigenmode :

$$\gamma_n(f) \triangleq \sqrt{(R_n + j\omega L_n)(G_n + j\omega C_n)} \tag{2.55}$$

$$= \alpha_n(f) + j\,\beta_n(f) = \alpha_n(f) + \frac{j\omega}{v_n(f)} \tag{2.56}$$

$$Z_{C_n}(f) \triangleq \sqrt{(R_n + j\omega L_n)\,/\,(G_n + j\omega C_n)} \tag{2.57}$$

Let us define the dielectric and conductor loss angles δ_d and $\delta_{c_n}(f)$ as follows:

$$\delta_d = \frac{G_n(f)}{\omega C_n} \qquad \delta_{c_n}(f) = \frac{R_n(f)}{\omega L_n} \tag{2.58}$$

The dielectric loss angle is a specific physical property depending on the dielectric type, while the conductor loss angle for the n-th mode is computed as follows:

$$\delta_{c_n}(f) = \frac{\sum_{k=0}^{N_c} \frac{R_{mk}(f)}{b} r_{nk}}{\omega\mu/c_n} = \frac{R_m(f)}{\omega\mu b}\, r_n\, c_n = \frac{\delta_{c_{n1}}}{\sqrt{f}} \tag{2.59}$$

where the unit-frequency conductor loss angle $\delta_{c_{n1}}$ is defined as :

$$\delta_{c_{n1}} \triangleq \frac{R_m(1)}{2\pi\mu b} r_n c_n. \tag{2.60}$$

Using these definitions, the propagation factor $\gamma_n(f)$ and the characteristic impedance $Z_{c_n}(f)$ can be expressed as :

$$\gamma_n(f) = \frac{\omega\sqrt{\kappa}}{c}\sqrt{(j+\delta_d)\left[(1+j)\,\delta_{c_n}(f) + j\right]} \tag{2.61}$$

$$Z_{C_n}(f) = \frac{Z_0}{\sqrt{\kappa}\, c_n}\sqrt{\frac{(1+j)\delta_{ci}(f) + j}{j + \delta_d}} \tag{2.62}$$

It can be shown that, when the losses are small, $(\delta_d, \delta_{c_n}(f)) \ll 1$, the lineic attenuation α_n, the phase velocity v_n and the characteristic impedance Z_{C_n} associated with the n-th mode are approximated by :

$$\alpha_n(f) \approx \frac{\omega\sqrt{\kappa}}{2c}\left[\delta_d + \delta_{c_n}(f)\right] \tag{2.63}$$

$$v_n(f) \approx \frac{c}{\sqrt{\kappa}}\left[\frac{1}{1 + \frac{\delta_{c_n}(f)}{2}}\right] \tag{2.64}$$

$$Z_{C_n}(f) \approx \frac{Z_0}{\sqrt{\kappa}\, c_n}\left[\left(1 + \frac{\delta_{c_n}(f)}{2}\right) + j\left(\frac{\delta_d - \delta_{c_n}(f)}{2}\right)\right] \tag{2.65}$$

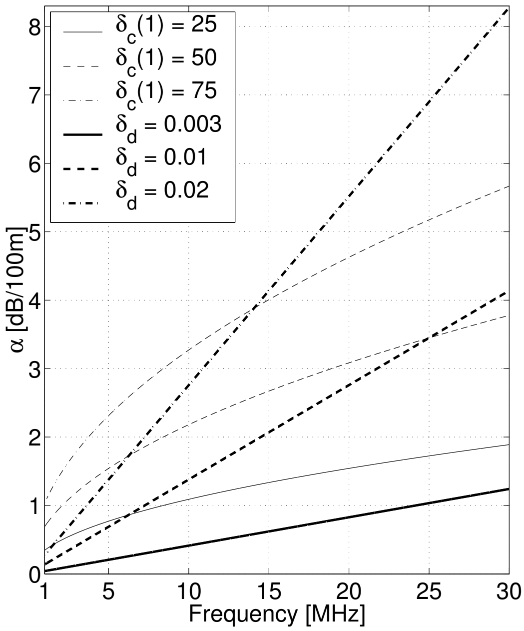

Figure 2.4: *Lineic attenuation α (in dB/100m) vs. frequency*

The phase velocity and characteristic impedance are approximately constant in the useful frequency range. The lineic attenuation α_n, however, varies quickly with the frequency. Figure 2.4 illustrates the evolution of $\alpha_n(f)$ in dB per 100 meter of cable, in the frequency range of 1 to 30 MHz. The bold curves give the contribution of dielectric losses for $\delta_d = \{0.003, 0.01, 0.02\}$, while the thin curves correspond to the conductor losses with $\delta_{c_1} = \{25, 50, 75\}$. As pointed out by equation (2.63), both contributions have to be added to obtain the global attenuation.

2.3.6 Examples

2.3.6.1 Symmetric 4-conductor cables

The first 2 schemes in Figure 2.3 give two kinds of highly symmetric cables with $N_c = 4$ internal conductors. Thanks to that symmetry, the derivation of the capacitance and resistance matrices (through the Laplace equation) involves 6 parameters $\{c_1, c_2, c_3\}$ and $\{r_1, r_2, r_3\}$ rather than $N_c^2 + N_c = 20$

parameters as in the general case :

$$\underline{\underline{C}}_w \propto \begin{bmatrix} c_1 & -c_2 & -c_3 & -c_2 \\ -c_2 & c_1 & -c_2 & -c_3 \\ -c_3 & -c_2 & c_1 & -c_2 \\ -c_2 & -c_3 & -c_2 & c_1 \end{bmatrix} \qquad \underline{\underline{R}}_w \propto \begin{bmatrix} r_1 & r_2 & r_3 & r_2 \\ r_2 & r_1 & r_2 & r_3 \\ r_3 & r_2 & r_1 & r_2 \\ r_2 & r_3 & r_2 & r_1 \end{bmatrix} \tag{2.66}$$

The eigenmodes are the same for both cable types (4 disks or 4 sectors as inner conductors). The line voltages are defined as follows:

$$\underline{V}_w = \begin{bmatrix} 1/2 & 0 & 1/2 & 1 \\ 0 & 1/2 & -1/2 & 1 \\ -1/2 & 0 & 1/2 & 1 \\ 0 & -1/2 & -1/2 & 1 \end{bmatrix} \underline{V}_L \tag{2.67}$$

$$\underline{V}_L = \begin{bmatrix} 1 & 0 & -1 & 0 \\ 0 & 1 & 0 & -1 \\ 1/2 & -1/2 & 1/2 & -1/2 \\ 1/4 & 1/4 & 1/4 & 1/4 \end{bmatrix} \underline{V}_w \tag{2.68}$$

The first two eigenmodes are the differential modes between opposite conductors, the third one is the phantom mode and the last one is the common mode. These eigenmodes are valid as long as the internal conductors are identical. Otherwise, the symmetry would be lost. The screen conductor, however, can be made from a different metal without modifying the definition of the eigenmodes. For the line voltages defined in equation (2.67), the capacitance and resistance coefficients are given by

$$\bar{c}_1 = \frac{1}{2}(c_1 + c_3) = \bar{c}_2 \qquad \bar{r}_1 = 2(r_1 + r_3) = \bar{r}_2 \tag{2.69}$$

$$\bar{c}_3 = c_1 - c_3 + 2c_2 \qquad \bar{r}_3 = r_1 - r_3 + 2r_2 \tag{2.70}$$

$$\bar{c}_4 = 4(c_1 - c_3 - 2c_2) \qquad \bar{r}_4 = \frac{1}{4}(r_1 - r_3 - 2r_2) \tag{2.71}$$

In Figure 2.2, the selected voltage configurations actually correspond to the 3 line voltages defined here. The figures illustrate the distribution of local currents/charges for a unit line voltage : by comparison, it can be observed that $\bar{c}_1 < \bar{c}_3 < \bar{c}_4$.

2.3.6.2 Symmetric 3-conductor cables

The third and fourth schemes in Figure 2.3 give two kinds of highly symmetric cables with $N_c = 3$ internal conductors. Here, 4 parameters $\{c_1, c_2\}$

and $\{r_1, r_2\}$ are required to obtain the resistance and capacitance matrices, rather than $N_c^2 + N_c = 12$ as in the general case :

$$\underline{\underline{C}}_w \propto \begin{bmatrix} c_1 & -c_2 & -c_2 \\ -c_2 & c_1 & -c_2 \\ -c_2 & -c_2 & c_1 \end{bmatrix} \qquad \underline{\underline{R}}_w \propto \begin{bmatrix} r_1 & r_2 & r_2 \\ r_2 & r_1 & r_2 \\ r_2 & r_2 & r_1 \end{bmatrix} \tag{2.72}$$

The line voltages corresponding to the eigenmodes can be defined as follows:

$$\underline{V}_w = \begin{bmatrix} 1/2 & 1/3 & 1 \\ 0 & -2/3 & 1 \\ -1/2 & 1/3 & 1 \end{bmatrix} \underline{V}_L \qquad \underline{V}_L = \begin{bmatrix} 1 & 0 & -1 \\ 1/2 & -1 & 1/2 \\ 1/3 & 1/3 & 1/3 \end{bmatrix} \underline{V}_w \tag{2.73}$$

The first two eigenmodes correspond to the same eigenvalue. The first one is defined as a 'phase-to-phase' mode between conductors 1 and 3, conductor 2 being hold at zero. The second one is defined as a 'symmetric mode' with equal voltages for conductors 1 and 3, conductor 2 getting the opposite polarity. The last one is the common mode. For the line voltages defined in equation (2.73), the capacitance and resistance coefficients are given by

$$\bar{c}_1 = \frac{1}{2}(c_1 + c_2) \qquad \bar{r}_1 = 2(r_1 - r_2) \tag{2.74}$$

$$\bar{c}_2 = \frac{2}{3}(c_1 + c_2) \qquad \bar{r}_2 = \frac{3}{2}(r_1 - r_2) \tag{2.75}$$

$$\bar{c}_3 = 3(c_1 - 2c_2) \qquad \bar{r}_3 = \frac{1}{3}(r_1 + 2r_2) \tag{2.76}$$

The coefficients associated with the first two eigenmodes are not independent.

2.3.6.3 Asymmetric 3-conductor cable

The last scheme of Figure 2.3 corresponds to a partly asymmetric cable. The external conductor is obtained by the concatenation of the circular screen and the neutral conductor in galvanic contact with the screen. The three internal conductors are no longer interchangeable. Here, the resolution of the Laplace equation finally provides 8 parameters $\{c_1, c_2, c_3, c_4\}$ and $\{r_1, r_2, r_3, r_4\}$:

$$\underline{\underline{C}}_w \propto \begin{bmatrix} c_1 & -c_2 & -c_3 \\ -c_2 & c_4 & -c_2 \\ -c_3 & -c_2 & c_1 \end{bmatrix} \qquad \underline{\underline{R}}_w \propto \begin{bmatrix} r_1 & r_2 & r_3 \\ r_2 & r_4 & r_2 \\ r_3 & r_2 & r_1 \end{bmatrix} \tag{2.77}$$

For this asymmetric configuration, the definition of the line voltages associated with the eigenmodes actually varies with the cable geometry. They can be expressed as follows :

$$\underline{V}_w = \begin{bmatrix} 1/2 & \frac{\bar{v}_2}{3} & 1 \\ 0 & -\frac{1-\bar{v}_2}{3} & \bar{v}_3 \\ -1/2 & \frac{\bar{v}_2}{3} & 1 \end{bmatrix} \underline{V}_L \tag{2.78}$$

$$\underline{V}_L = \begin{bmatrix} 1 & 0 & -1 \\ \frac{\bar{v}_3}{2\bar{v}_{23}} & \frac{-1}{\bar{v}_{23}} & \frac{\bar{v}_3}{2\bar{v}_{23}} \\ \frac{1-\bar{v}_2/3}{2\bar{v}_{23}} & \frac{\bar{v}_2/3}{\bar{v}_{23}} & \frac{1-\bar{v}_2/3}{2\bar{v}_{23}} \end{bmatrix} \underline{V}_w \tag{2.79}$$

with $\bar{v}_{23} \triangleq 1 + \frac{\bar{v}_2}{3}(\bar{v}_3 - 1)$. In the 'line voltage' formulation, the solution is then fully defined by the 8 parameters $\{\bar{c}_1, \bar{c}_2, \bar{c}_3\}$, $\{\bar{r}_1, \bar{r}_2, \bar{r}_3\}$ and $\{\bar{v}_2, \bar{v}_3\}$. For a given geometrical setup (as the last scheme of Figure 2.3 for instance), those 8 parameters only depend on the ratio a/b. The first mode is the phase-to-phase mode, the second one is a 'modified' symmetric mode parametrized by $\bar{v}_2$, and the last one is a 'modified' common mode parametrized by $\bar{v}_3$. The last two eigenmodes are the same as in the symmetric case for $\bar{v}_2 = 1$ and $\bar{v}_3 = 1$, respectively.

2.3.6.4 Computational results

Figures 2.5 and 2.6 give the evolution of the computed geometrical parameters with the ratio a/b, for each of the 5 types of cables proposed in Figure 2.3 and for each line voltage as given by equations (2.67), (2.73) and (2.79). The left part of the figures gives the product $\bar{c}_n \bar{r}_n$ for each eigenmode, which determines the conductor loss angle $\delta_{c_n}(f)$ as given by (2.59). The right part of the figures gives the ratio $Z_0/\bar{c}_n$ for each eigenmode, which determines the characteristic impedance $Z_{C_n}(f)$ as given by (2.62).

For the purpose of comparison, equivalent parameters are also represented for a standard coax cable with dimensions a and b. The geometrical parameters $\bar{c}_n$ and $\bar{r}_n$ are given by (2.52) for the coax cable ('line' voltages are equivalent to 'wire' voltages as $N_c = 1$).

Finally, Figure 2.7 gives the parameters $\bar{v}_2$ and $\bar{v}_3$, which determine the definition of the line voltages for the asymmetric cable as given by (2.79).

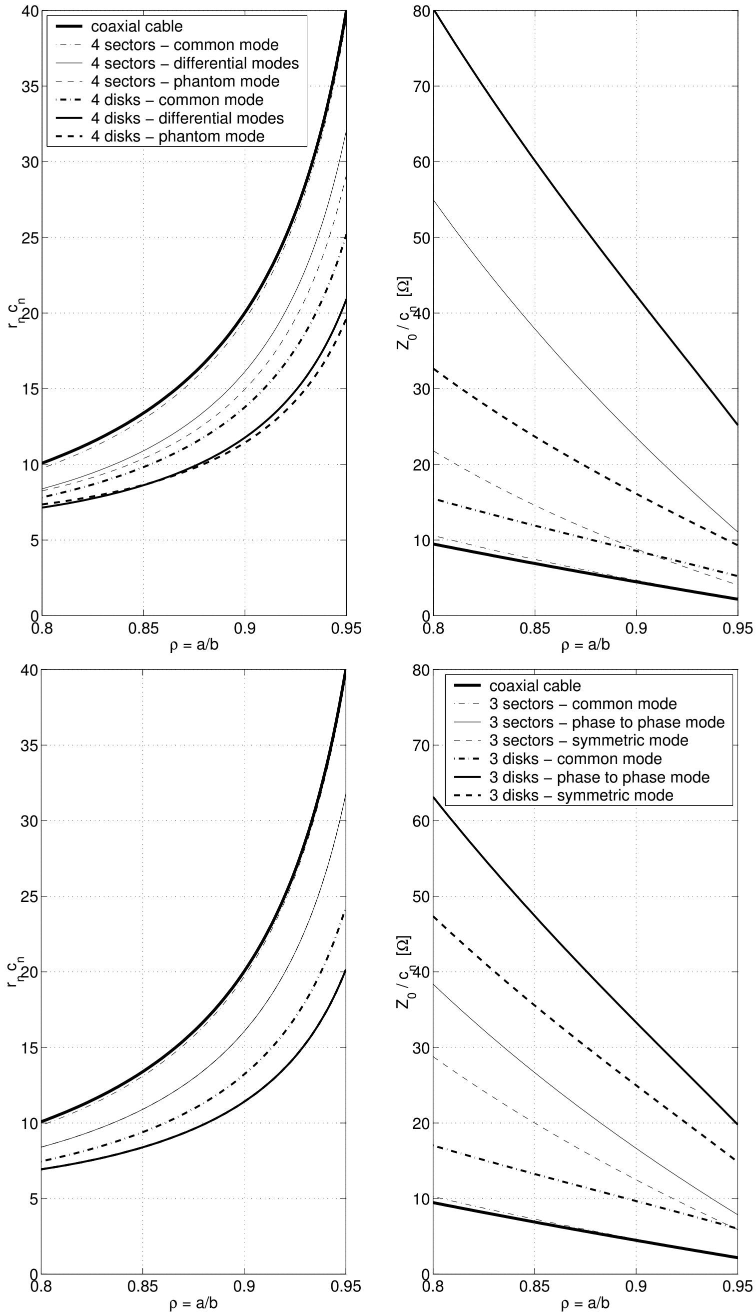

Figure 2.5: *$\bar{r}_n\bar{c}_n$ and $Z_0/\bar{c}_n$ computed for symmetric cables with 4 and 3 conductors*

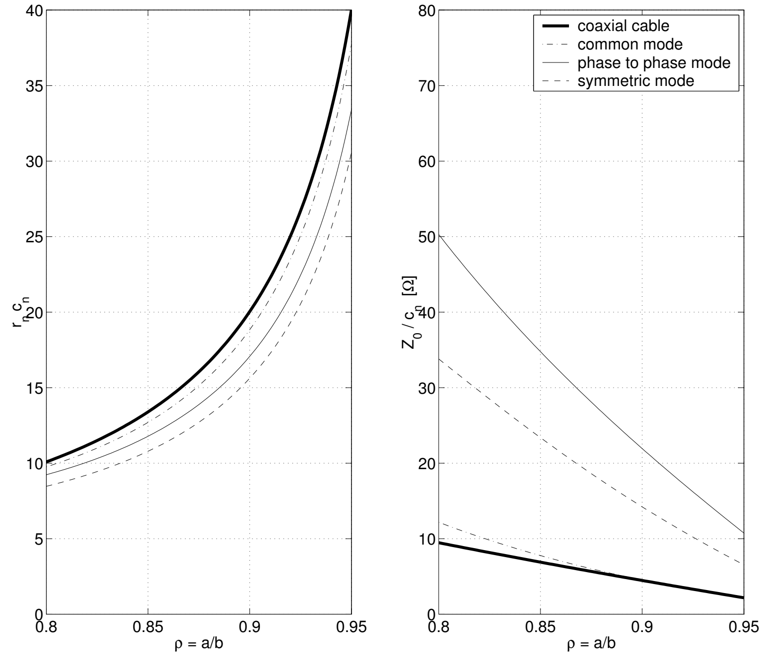

Figure 2.6: *$\bar{r}_n\bar{c}_n$ and $Z_0/\bar{c}_n$ computed for the 3 sector + 1 disk cable*

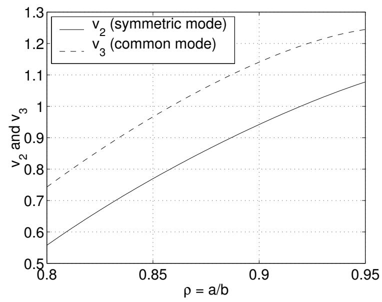

Figure 2.7: *Eigenmode parameters computed for the 3 sector + 1 disk cable*

2.3.7 Practical PLC cables

Table 2.1 gives the main characteristics of 5 PLC cables which are representative of the cables used in the underground power distribution network. The cable dimensions b and a/b are given in the table, and comparative drawings of the cable cross-sections are displayed above the table. Copper ($\sigma = 56.10^6\mathrm{m}^{-1}\Omega^{-1}$) or aluminium ($\sigma = 35.10^6\mathrm{m}^{-1}\Omega^{-1}$) is used for the conductors. In the case of the asymmetric cable, the composite external conductor is made of steel (screen) and lead (neutral conductor). Two types of dielectric material are currently used in the PLC cables : polyvinylchloride (PVC) with $\kappa \approx 3.3$ and $\delta_d \approx 0.03$, and polyethylene (PE) with $\kappa \approx 2.3$ and $\delta_d \approx 0.003$. The unit-frequency conductor loss angle $\delta_{c_{n1}}$ and the impedance characteristic $Z_{c_n} \approx \frac{Z_0}{\sqrt{\kappa \bar{c}_n}}$ is given for each eigenmode. The first 3 types cables will be used in Section 2.5 for the simulation of a realistic PLC access network.

2.4 Impulse response associated with a cable segment

The object of this section is to analyze the channel impulse response $h(t, L)$ associated with a simple cable segment of length L.

Using the cable model developed in section 2.3.5, the cable impulse response can be expressed as the convolution of three components :

$$h(t, L) \approx \delta(t - \Delta) \otimes h_c(t, L) \otimes h_d(t, L) \tag{2.80}$$

where $\Delta \triangleq L/v$ is the propagation time corresponding to a cable length L and a wave velocity v. These components reflect specific physical mechanisms :

- $\delta(t - \Delta)$ represents a simple propagation delay, it gives the channel impulse response that would be associated with a perfect (lossless) cable

- $h_c(t, L) = \mathcal{F}^{-1}\{H_c(\omega, L)\}$ with $H_c(\omega, L) \triangleq e^{-\sqrt{j\omega}\,\sqrt{\pi}\,\delta_{c1}\Delta}$ represents the effect of conductor losses

- $h_d(t, L) = \mathcal{F}^{-1}\{H_d(\omega, L)\}$ with $H_d(\omega, L) \triangleq e^{-\omega\,\delta_d\Delta/2}$ represents the effect of dielectric losses

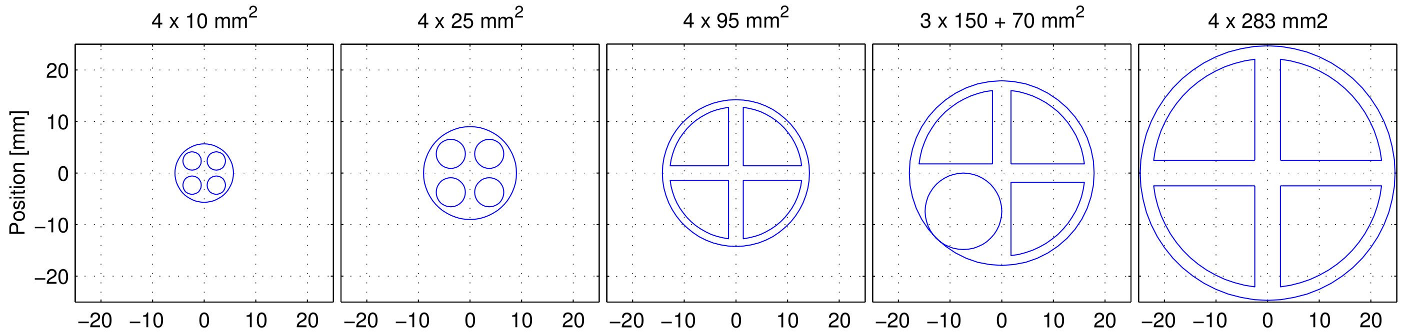

Name	Conductors (in/out)	b [mm]	$\frac{a}{b}$	Differential		Phantom		Common	
				δ_{c_1} [$\sqrt{\text{Hz}}$]	Z_c [Ω]	δ_{c_1} [$\sqrt{\text{Hz}}$]	Z_c [Ω]	δ_{c_1} [$\sqrt{\text{Hz}}$]	Z_c [Ω]
4×10	Cu	5.7	0.9	69.9	39.4	67.9	15.0	81.8	8.0
4×25	Cu	9	0.9	44.0	39.4	42.8	15.0	41.5	8.0
4×95	Alu	14	0.9	48.3	21.9	44.8	8.2	58.6	4.4
4×150	Alu	18	0.9	38.4	21.9	35.6	8.2	46.6	4.4
$3 \times 150 + 70$	Alu/Steel-Pb	18	0.9	45.9	21.9	40.9	14.2	51.6	4.6
4×283	Cu/Alu	25	0.9	24.0	21.9	21.9	8.2	30.0	4.4

Table 2.1: *Cross-section, conductors, geometrical dimensions and computed conductor losses and characteristic impedance of some powerline cables*

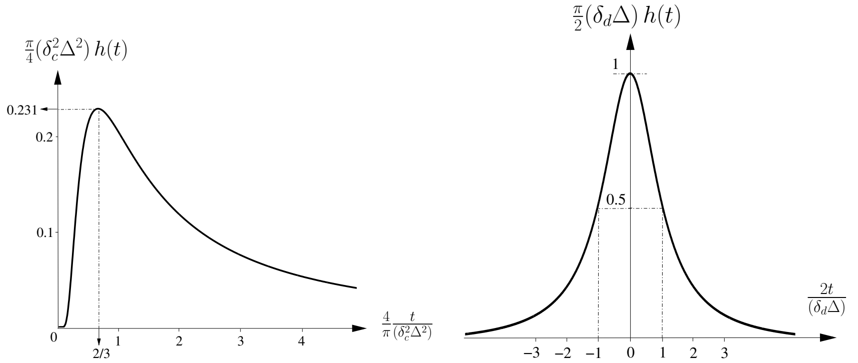

Figure 2.8: *Normalized pulses $K_c h_c(t,L)$ and $\pi K_d h_d(t,L)$*

Applying the inverse Fourier transform $\mathcal{F}^{-1}(.)$ to the partial frequency responses given above, explicit expressions of $h_c(t,L)$ and $h_d(t,L)$ can be obtained as follows [35][36] :

$$h_c(t,L) = \left(\frac{1}{K_c}\right)\frac{e^{\frac{-1}{\tau_c}}}{\sqrt{\pi\tau_c^3}} \tag{2.81}$$

$$h_d(t,L) = \left(\frac{1}{\pi K_d}\right)\frac{1}{\tau_d^2+1} \tag{2.82}$$

with the constant parameters $K_c \triangleq \frac{\pi}{4}(\delta_{c1}\Delta)^2$ and $K_d \triangleq \frac{\delta_d\Delta}{2}$, and the normalized time variables $\tau_c = t/K_c$ and $\tau_d = t/K_d$.

Figure 2.8 illustrates the normalized impulse responses $K_c h_c(t,L)$ and $\pi K_d h_d(t,L)$ in the ranges $\tau_c \in [0,5]$ and $\tau_d \in [-5,5]$, respectively. From the definitions given in (2.81)-(2.82), it appears that the length (resp. the maximum) of the partial impulse responses are proportional (resp. inversely proportional) to the squared product $(\delta_{c1}\Delta)^2$ for the conductor losses, and to the product $(\delta_d\Delta)$ for the dielectric losses. This gives an indication about how the shape of the cable impulse response varies with the cable length $L = \Delta v$.

An important remark should be made here concerning the validity of our dielectric model. The impulse response $h_d(t,L)$ derived above is obviously non-causal : it can not correspond to a physical process. The reason of this lies in the extreme simplicity of the dielectric model :

$$\varepsilon(\omega) = \varepsilon' - j\varepsilon" \qquad \forall\omega. \tag{2.83}$$

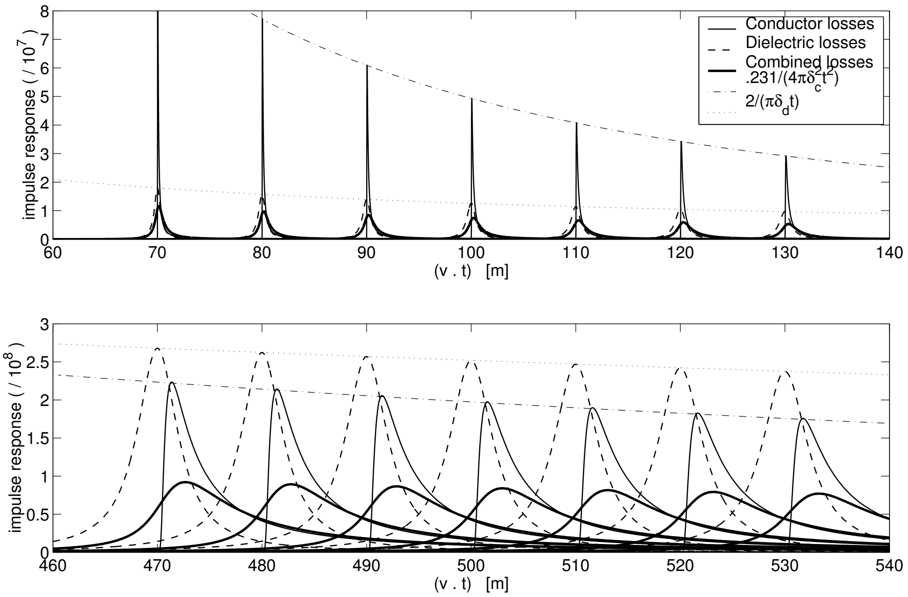

Figure 2.9: *Impulse responses for different cable lengths ($\delta_{c_1} = 48$, $\delta_d = 0.01$, $\kappa = 2.3$) around 100 m (up) and around 500 m (down)*

This is in contradiction with the Kronig and Kramers property [37] specifying that *"a dissipative material (ε" $\neq 0$) must be dispersive (ε varies with ω), and inversely"*. A valid dielectric model should include the variability of the dielectric properties in the useful frequency range, which is not the case here. However, the simple dielectric model proposed above offers a good approximation, even if the causality constraint is not satisfied. In particular, we have that $h_d(-\Delta)/h_d(0) \approx \delta_d^2/2 \ll 1$, which guarantees that the non-causal part of the impulse response is negligible if the propagation delay Δ is taken into account.

Figure 2.9 gives the (non-normalized) impulse responses $h_c(t-\Delta, L)$ (thin solid lines), $h_d(t-\Delta, L)$ (dashed lines) and $(h_c \otimes h_d)(t-\Delta, L)$ (bold solid lines) corresponding to various cable lengths around 100 meter (upper figure) and around 500 meter (lower figure). This allows the comparison of the respective influences of conductor and dielectric losses on the shape of the composite impulse response, as well as the evolution of this shape with the cable length.

The surface under the impulses $h_c(t, L)$ and $h_d(t, L)$ is independent of the cable length as

$$\int_{-\infty}^{+\infty} h_c(t, L)\ \mathrm{d}t = \int_{-\infty}^{+\infty} h_d(t, L)\ \mathrm{d}t = 1 \quad \forall L. \tag{2.84}$$

This unit value actually corresponds to the channel gain at a zero frequency $H_c(0)$ or $H_d(0)$. It should be reminded, however, that the propagation model derived here is only valid at high frequency (i.e. when the skin depth is small with respect to the conductor dimensions). The property considered here is then just a consequence of the propagation model extrapolation to the zero-frequency, and does not reflect a physical reality. But this approximation is acceptable in our context as the impulse responses studied here are going to be used in relation with passband signals only.

The energy of these impulses can be computed as :

$$\int_{-\infty}^{+\infty} h_c^2(t, L)\ \mathrm{d}t = \frac{1}{4\pi K_c} \tag{2.85}$$

$$\int_{-\infty}^{+\infty} h_d^2(t, L)\ \mathrm{d}t = \frac{1}{2\pi K_d} \tag{2.86}$$

These relations show that full-band signals transmitted on the cable would lose their energy proportionally to the cable length L (as far as the dielectric losses are concerned) or proportionally to the square of the cable length L^2 (as far as the conductor losses are concerned). The effective combined loss would be intermediate. Actually these conclusions are only valid asymptotically for large values of L as the real signals that will be transmitted on the cable have a limited bandwidth.

The effect of a cable segment of length L on a unit-energy band-limited pulse $p(t, T)$ of bandwidth $B = \frac{0.5}{T}$ would be more informative. That is what we propose to analyze now. Let $r(t, T, L)$ be the signal received after propagation over the cable segment, i.e. :

$$r(t, T, L) = p(t - \Delta, T) \otimes h_c(t, L) \otimes h_d(t, L) \tag{2.87}$$

The energy of the received signal is given by

$$\mathcal{E}_{cd}\,(T, L) \triangleq 2T \int_0^{\frac{0.5}{T}} |H_c(f)\,.H_d(f)|^2 \mathrm{d}f \tag{2.88}$$

Analytical results can be easily obtained by studying separately the dielectric and conductor effects :

$$\mathcal{E}_c\left(T,L\right) \triangleq 2T\int_0^{\frac{0.5}{T}} |H_c(f)|^2 \mathrm{d}f \qquad = \frac{2}{\rho_c^2}\left(1-e^{-\rho_c}\right) - \frac{2}{\rho_c}e^{-\rho_c} \tag{2.89}$$

$$\mathcal{E}_d\left(T,L\right) \triangleq 2T\int_0^{\frac{0.5}{T}} |H_d(f)|^2 \mathrm{d}f \qquad = \frac{1}{\rho_d}\left(1-e^{-\rho_d}\right) \tag{2.90}$$

with $\rho_c \triangleq \frac{\pi\delta_{c1}\Delta}{\sqrt{T/2}}$ and $\rho_d \triangleq \frac{\pi\delta_d\Delta}{T}$.

Figure 2.10 (left part) gives the logarithmic energy losses (in dB) for cable lengths in the range of 0 to 2000 meter and a baseband pulse of 10 MHz bandwidth. The solid curves represent the dielectric losses, the conductor losses and the combined losses as given by equations (2.90), (2.89) and (2.88), respectively. The dashed curves (straight lines) correspond to the asymptotic behavior for very short cables. Both types of losses are then cumulative :

$$\mathcal{E}_{cd}(T,L) \approx \mathcal{E}_c(T,L).\mathcal{E}_d(T,L) \approx 1 - \frac{2}{3}\rho_a - \frac{1}{2}\rho_b, \tag{2.91}$$

which corresponds to a global loss of

$$\frac{-10}{\log(10)}\frac{\pi}{v}\left(\frac{2}{3}\frac{\delta_{c1}}{\sqrt{T/2}} + \frac{1}{2}\frac{\delta_d}{T}\right) \qquad [\mathrm{dB/m}]$$

This approximation is valid for short distances (up to a few tens of meter). The dashed-dotted curves correspond to the asymptotic behavior for long cables. The respective losses increase then by 10 dB/decade ($\mathcal{E}_d$) and 20 dB/decade ($\mathcal{E}_c$), and the global loss is dominated by the contribution of conductor losses.

Finally, the effect of a cable segment on a passband pulse should be taken into consideration, as the lower part of the frequency spectrum is not available for the transmission of PLC signals. Assuming a unit-energy passband pulse $\sqrt{2}\,p(t,T)\cos(\omega_c t)$ with a useful bandwidth $[B_1, B_2] = [0.5/T_1, 0.5/T_2]$, the energy of the received signal can be obtained by

$$\bar{\mathcal{E}}_{cd}\left(T_1,T_2,L\right) = \frac{T_1}{T_1-T_2}\mathcal{E}_{cd}\left(T_2,L\right) - \frac{T_2}{T_1-T_2}\mathcal{E}_{cd}\left(T_1,L\right). \tag{2.92}$$

The right part of Figure 2.10 gives the logarithmic energy losses (in dB) for a passband pulse in the 1 Mhz - 10 MHz band and different combinations of cable properties ($\delta_d = 0.003$, 0.01 and 0.02, $\delta_{c1} = 25$, 50 and 75).

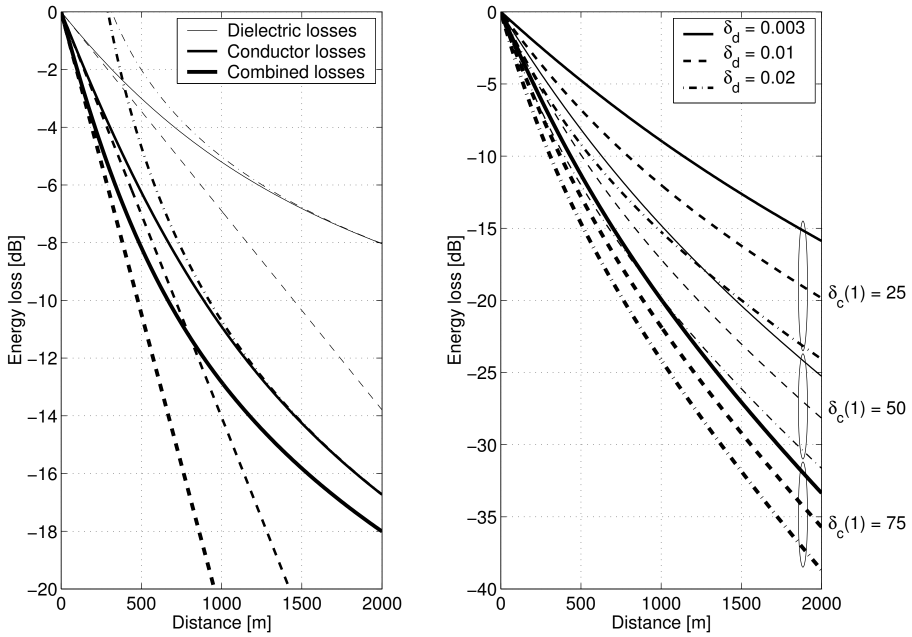

Figure 2.10: *Energy loss vs. distance. Left: relative effects of dielectric and conductor losses ($\delta_{c_1} = 50$, $\delta_d = 0.01$), and asymptotic behavior, with a baseband pulse. Right: energy loss for different combinations of δ_{c_1} and δ_d, with a passband pulse.*

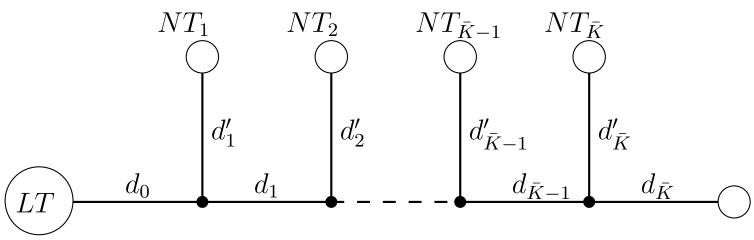

Figure 2.11: *Wireline multiaccess network*

2.5 Powerline access networks

Underground powerline access networks generally consist of a main *distribution cable* starting at the medium-voltage low-voltage transformer, and lying below the streets with *derivation cables* providing the final connection to the various subscriber buildings. Broadband modems (Network Terminations or NTs) may be connected on these termination points, just before the power meter, and tranmit and/or receive digital signals to/from the central office (Line Termination or LT). Evaluation of the communication link performance requires the knowledge of the end-to-end channel response. This global channel is the concatenation of several cable segments, and must take into account the presence of cable derivations and the various loads connected to the termination points.

Figure 2.11 illustrates the general access network topology, where d_k and d'_k denote the length of the different cable segments.
Many variations of the general prototype presented in Figure 2.11 could be investigated and analyzed, leading to different classes of powerline channel models. Many items have to be taken into consideration in the derivation of the channel model :

- The total number of derivations $\bar{K}$.
- The position of the $K \leq \bar{K}$ user modems along the distribution cable. The $\bar{K}-K$ remaining derivations correspond to simple power delivery points, without PLC access.
- The length of the different cable segments (d_k and d'_k).
- The nature of the different cables : number of conductors, definition of the eigenmodes, propagation parameters $(v, \delta_{c1}, \delta_d)$ and characteristic impedance Z_c for each mode.

- The structure of the derivation points (conductors interconnections).
- The nature of termination points (matched, open, other).

Our objective is not to give an exhaustive set of different PLC channel models, but rather to develop a detailed analysis of a representative example and to analyze the influence of some key parameters on the resulting channel responses.

The selected example is depicted in Figure 2.12. The proposed access network includes a 300 m distribution cable and $\bar{K} = 20$ derivations. A central office modem (LT) is located at the medium-voltage low-voltage transformer, and 5 user modems (NTs) are located at selected customer premises, as suggested on the figure. The distribution cable is supposed to be of aluminium with $4 \times 95\,\mathrm{mm}^2$ sectors, and the derivation cables are supposed to be of copper with $4 \times 25\,\mathrm{mm}^2$ or $4 \times 10\,\mathrm{mm}^2$ disks in the cross-section. The cable segments have a length in the set $\{5, 10, 15, 20, 25, 30, 35\}$ meter (the different values can be determined unambiguously from the figure). The main information relative to the position of the 5 NTs is summarized in the following table :

NT	Position k	$\sum_{l=0}^{k-1} d_l$ [m]	d'_k [m]	Total distance [m]
1	2	15	10	25
2	5	60	15	75
3	10	140	35	175
4	15	220	5	225
5	20	290	20	310

Table 2.2: *Position of the 5 NTs, and distance from the LT*

The three types of cables used here have identical eigenmodes (differential, phantom and common), but specific propagation parameters and characteristic impedances. Ideal connections between the respective cable conductors are assumed at the derivation points, which guarantees that the signals associated to each eigenmode do not mix to each other at these points. The termination points at modem locations (LT and 5 NTs) are assumed to be perfectly matched, simultaneously in the different eigenmodes. Finally the 16 remaining termination points are assumed to have an intermediate impedance, between open and matched.

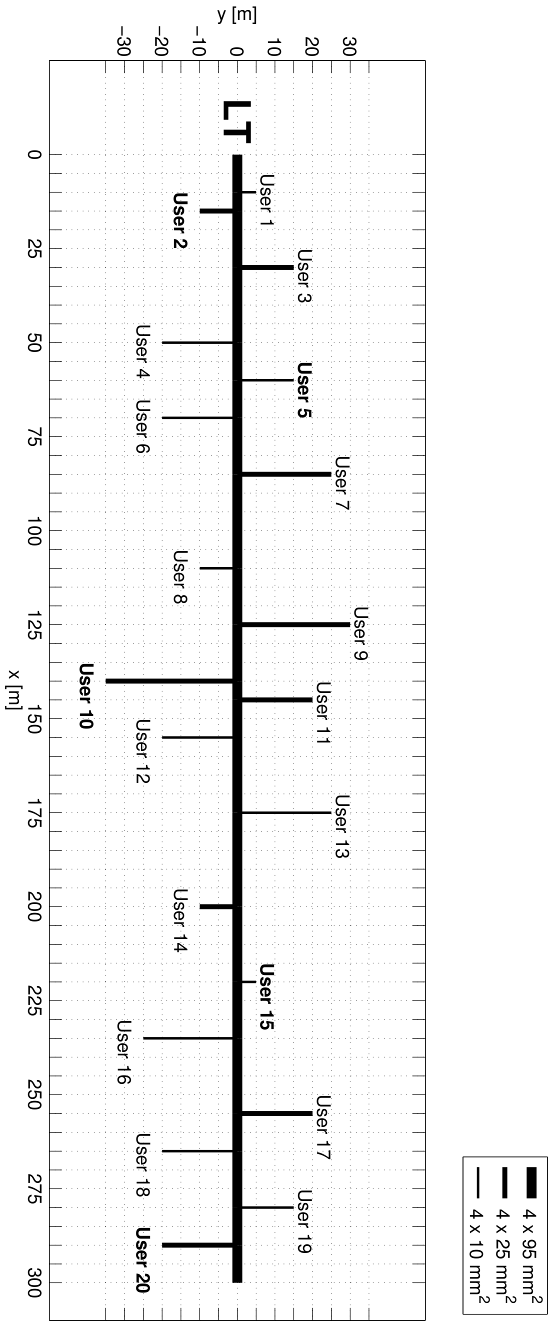

Figure 2.12: *A small powerline access network*

2.6 Network analysis based on the scattering matrix

2.6.1 The scattering matrix

The different elements constituting the low voltage access network may be modeled as 2N-port modules characterized by their multidimensional scattering matrix $\underline{\underline{S}}$, that links the outgoing waves $(\underline{B}_1, \underline{A}_2)$ to the incoming waves $(\underline{A}_1, \underline{B}_2)$. Grouping together adjacent elements of the network leads to the cascading of the corresponding scattering matrices. A specific algebra for the combination of multidimensional scattering matrices has to be developed, taking into account the joint presence of cables with a different number of conductors. Assuming a given scattering matrix $\underline{\underline{S}}_x$ with N_1-fold inputs and N_2-fold outputs, to be cascaded with a given scattering matrix $\underline{\underline{S}}_y$ with N_2-fold inputs and N_3-fold outputs. The building blocks of the resulting scattering matrix $\underline{\underline{S}}$ are given by :

$$
\begin{aligned}
\underline{\underline{S}}_{11} &= \underline{\underline{S}}_{11}^T = \underline{\underline{S}}_{x,11} + \underline{\underline{S}}_{x,12}\left(\underline{\underline{E}}_{N_2} - \underline{\underline{S}}_{y,11}\,\underline{\underline{S}}_{x,22}\right)^{-1}\underline{\underline{S}}_{y,11}\,\underline{\underline{S}}_{x,21} \\
\underline{\underline{S}}_{12} &= \underline{\underline{S}}_{21}^T = \underline{\underline{S}}_{x,12}\left(\underline{\underline{E}}_{N_2} - \underline{\underline{S}}_{y,11}\,\underline{\underline{S}}_{x,22}\right)^{-1}\underline{\underline{S}}_{y,12} \\
\underline{\underline{S}}_{22} &= \underline{\underline{S}}_{22}^T = \underline{\underline{S}}_{y,22} + \underline{\underline{S}}_{y,21}\left(\underline{\underline{E}}_{N_2} - \underline{\underline{S}}_{x,22}\,\underline{\underline{S}}_{y,11}\right)^{-1}\underline{\underline{S}}_{x,22}\,\underline{\underline{S}}_{y,12}
\end{aligned}
\tag{2.93}
$$

On the other hand, the transfer of a size-N_2 reflection matrix $\underline{\underline{K}}_{\text{out}}$ through a scattering matrix $\underline{\underline{S}}$ with N_1-fold inputs and N_2-fold outputs provides a size-N_1 reflection matrix $\underline{\underline{K}}_{\text{in}}$ as follows :

$$
\underline{\underline{K}}_{\text{in}} = \underline{\underline{S}}_{11} + \underline{\underline{S}}_{12}\left(\underline{\underline{E}}_{N_2} - \underline{\underline{K}}_{\text{out}}\,\underline{\underline{S}}_{22}\right)^{-1}\underline{\underline{K}}_{\text{out}}\,\underline{\underline{S}}_{21}. \tag{2.94}
$$

Figure 2.13 illustrates the various waves and submatrices involved in equations (2.93) and (2.94).

2.6.2 Reference basis and matrix base change

A given scattering matrix $\underline{\underline{S}}$ depends on the definition of the waves $\underline{A}$ and $\underline{B}$ as a function of the line voltages and currents $\underline{V}$ and $\underline{I}$. Actually, any change of variables, from the pair $(\underline{V}, \underline{I})$ to the pair $(\underline{A}, \underline{B})$ may be investigated :

$$
\underline{V}(z) = \underline{\underline{U}}\,[\underline{A}(z) + \underline{B}(z)] \qquad \underline{I}(z) = \underline{\underline{J}}\,[\underline{A}(z) - \underline{B}(z)] \tag{2.95}
$$

where $\underline{\underline{U}}$ has the dimensions of the square root of an impedance, and the normalization condition $\underline{\underline{U}}^T\,\underline{\underline{J}} = \underline{\underline{E}}_N$ is satisfied. With these conditions, the

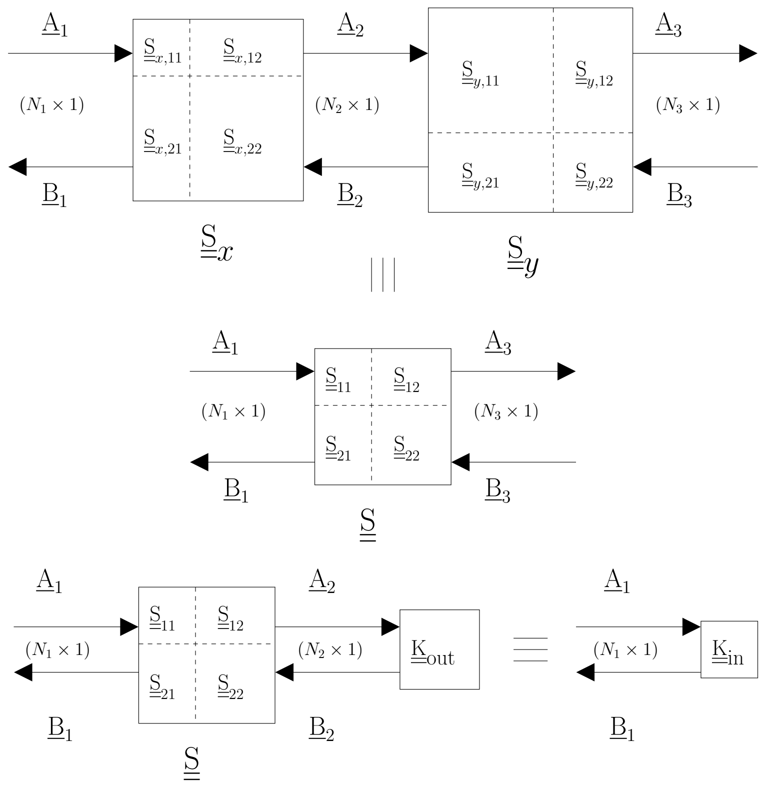

Figure 2.13: *Cascading scattering matrices*

dimension of the waves $\underline{A}$ and $\underline{B}$ in (2.95) is the square root of a power. The choice of modal matrices as in equation (2.40) results in the definition of eigenmodes, where the waves propagate with their own exponential propagation factor, but other choices are possible. A reference basis $(\underline{\underline{U}}_R, \underline{\underline{J}}_R)$ may be defined and used throughout the network. Different reference bases need to be defined for different parts of the network if the number of conductors varies from ones cable segment to another. It is then useful to develop equations for a base change, i.e. the relations between waves $(\underline{A}_x, \underline{B}_x)$ defined in a base $(\underline{\underline{U}}_x, \underline{\underline{J}}_x)$, and waves $(\underline{A}_y, \underline{B}_y)$ defined in another base $(\underline{\underline{U}}_y, \underline{\underline{J}}_y)$. The solution is expressed with a scattering matrix formalism as :

$$\left[\begin{array}{c} \underline{\underline{B}}_x \\ \underline{\underline{A}}_y \end{array}\right] = \left[\begin{array}{cc} (\underline{\underline{\Sigma}}_{xy})_{11} & (\underline{\underline{\Sigma}}_{xy})_{12} \\ (\underline{\underline{\Sigma}}_{xy})_{12}^T & (\underline{\underline{\Sigma}}_{xy})_{22} \end{array}\right] \left[\begin{array}{c} \underline{\underline{A}}_x \\ \underline{\underline{B}}_y \end{array}\right] \tag{2.96}$$

with the following submatrices :

$$\begin{aligned} (\underline{\underline{\Sigma}}_{xy})_{11} &= (\underline{\underline{z}}_{yx} + \underline{\underline{E}})^{-1}(\underline{\underline{z}}_{yx} - \underline{\underline{E}}) = (\underline{\underline{\Sigma}}_{yx})_{22} \\ (\underline{\underline{\Sigma}}_{xy})_{22} &= (\underline{\underline{z}}_{xy} + \underline{\underline{E}})^{-1}(\underline{\underline{z}}_{xy} - \underline{\underline{E}}) = (\underline{\underline{\Sigma}}_{yx})_{11} \\ (\underline{\underline{\Sigma}}_{xy})_{12} &= 2(\underline{\underline{z}}_{yx} + \underline{\underline{E}})^{-1} \underline{\underline{J}}_x^T \underline{\underline{U}}_y = (\underline{\underline{\Sigma}}_{yx})_{21} \end{aligned} \tag{2.97}$$

and $\underline{\underline{z}}_{yx} = \underline{\underline{J}}_x^T \underline{\underline{U}}_y \underline{\underline{U}}_y^T \underline{\underline{J}}_x = \underline{\underline{z}}_{yx}^T$, $\underline{\underline{z}}_{xy} = \underline{\underline{J}}_y^T \underline{\underline{U}}_x \underline{\underline{U}}_x^T \underline{\underline{J}}_y = \underline{\underline{z}}_{xy}^T$.

2.6.3 Cable segments

In the eigenbase $(\underline{\underline{U}}_0, \underline{\underline{J}}_0)$ of the cable, the scattering matrix representing a cable segment of length L is:

$$\underline{\underline{S}}_0 = \left[\begin{array}{cc} \underline{\underline{0}}_N & \underline{\underline{T}} \\ \underline{\underline{T}} & \underline{\underline{0}}_N \end{array}\right] \tag{2.98}$$

with $\underline{\underline{T}} = \mathrm{Diag}\left[\exp(-\gamma_n L)\right]$.

It is useful to express the scattering matrix $\underline{\underline{S}}_R$ of the cable segment in accordance with the chosen reference basis $\underline{\underline{U}}_R, \underline{\underline{J}}_R$. This is obtained by left- and right- cascading the initial matrix $\underline{\underline{S}}_0$ with the matrix base changes $\underline{\underline{\Sigma}}_{R0}$ and $\underline{\underline{\Sigma}}_{0R}$, respectively. The result is :

$$\begin{aligned} (\underline{\underline{S}}_R)_{11} = (\underline{\underline{S}}_R)_{22} = (\underline{\underline{\Sigma}}_{R0})_{11} + (\underline{\underline{\Sigma}}_{R0})_{12}\,\underline{\underline{T}} & \\ \left[\underline{\underline{E}}_N - (\underline{\underline{\Sigma}}_{R0})_{22}\,\underline{\underline{T}}\,(\underline{\underline{\Sigma}}_{R0})_{22}\,\underline{\underline{T}}\right]^{-1} & (\underline{\underline{\Sigma}}_{R0})_{22}\,\underline{\underline{T}}\,(\underline{\underline{\Sigma}}_{R0})_{21} \end{aligned} \tag{2.99}$$

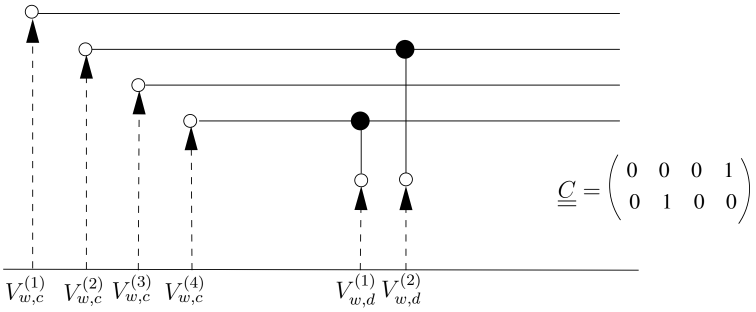

Figure 2.14: *Example of conductors interconnection and associated connection matrix*

$$(\underline{\underline{S}}_R)_{12} = (\underline{\underline{S}}_R)^T_{21} = (\underline{\underline{\Sigma}}_{R0})_{12}\,\underline{\underline{T}} \left[\underline{\underline{E}}_N - (\underline{\underline{\Sigma}}_{R0})_{22}\,\underline{\underline{T}}\,(\underline{\underline{\Sigma}}_{R0})_{22}\,\underline{\underline{T}}\right]^{-1} (\underline{\underline{\Sigma}}_{R0})_{21} \qquad (2.100)$$

2.6.4 Cable derivations

Assume a main distribution cable with N wires, a reference basis $(\underline{\underline{U}}_c, \underline{\underline{J}}_c)$, and line voltages defined by $\underline{\underline{N}}_c$. At a given point, a derivation cable with n wires, a reference basis $(\underline{\underline{U}}_d, \underline{\underline{J}}_d)$, and line voltages defined by $\underline{\underline{N}}_d$, is connected to it. Let us define a $n \times N$ connection matrix $\underline{\underline{C}}$ giving the wire connections between the main cable and the derivation cable :

$$\underline{V}_{w,d} = \underline{\underline{C}}\,\underline{V}_{w,c} \qquad (2.101)$$

where the entries of $\underline{\underline{C}}$ are 0's and 1's. Figure 2.14 gives an example of a matrix connection with $N = 4$ and $n = 2$. By its definition, the matrix connection satisfies the relation $\underline{\underline{C}}\,\underline{\underline{C}}^T = \underline{\underline{E}}_n$. We also define a modified connection matrix $\underline{\underline{D}}$ as follows :

$$\underline{\underline{D}} = \underline{\underline{J}}_d^T\,\underline{\underline{N}}_d^{-1}\,\underline{\underline{C}}\,\underline{\underline{N}}_c\,\underline{\underline{U}}_c \qquad (2.102)$$

The derivation point actually corresponds to a 3-port network. We need to compute the scattering matrix obtained when one of the ports is connected to a known charge.
In figure 2.15, the charge is supposed to be connected on the derivation side. The transmission along the main cable is given by :

$$\begin{array}{lllll} \underline{\underline{S}}_{11} & = & \underline{\underline{S}}_{22} & = & \underline{\underline{T}} \\ \underline{\underline{S}}_{12} & = & \underline{\underline{S}}_{21} & = & \underline{\underline{E}}_N + \underline{\underline{T}} \end{array} \qquad (2.103)$$

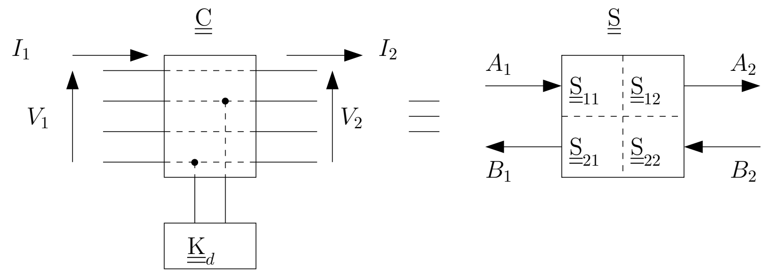

Figure 2.15: *Scattering matrix associated with a derivation (transmission along the distribution cable)*

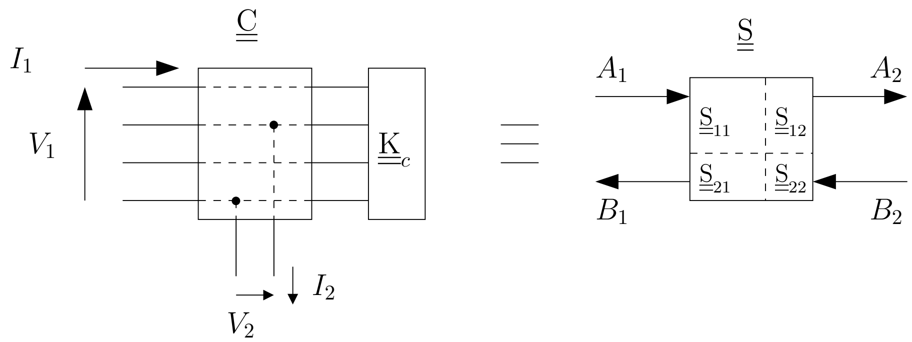

Figure 2.16: *Scattering matrix associated with a derivation (transmission from the distribution cable to the derivation cable)*

$$\underline{\underline{T}} = \underline{\underline{D}}^T \left(\underline{\underline{K}}_d - \underline{\underline{E}}_n\right) \left[\underline{\underline{D}}\,\underline{\underline{D}}^T \left(\underline{\underline{E}} - \underline{\underline{K}}_d\right) + 2\left(\underline{\underline{E}}_n + \underline{\underline{K}}_d\right)\right]^{-1} \underline{\underline{D}} \tag{2.104}$$

In figure 2.16, the charge is supposed to be connected on the main cable right side. The transmission from the main cable to the derivation cable is then given by :

$$\begin{aligned}\underline{\underline{S}}_{11} = \underline{\underline{S}}_{11}^T = \underline{\underline{K}}_c - \left(\underline{\underline{E}}_N + \underline{\underline{K}}_c\right) \underline{\underline{D}}^T \\ \left[\underline{\underline{D}}\left(\underline{\underline{E}}_N + \underline{\underline{K}}_c\right)\underline{\underline{D}}^T + 2\,\underline{\underline{E}}_n\right]^{-1} \underline{\underline{D}}\left(\underline{\underline{E}}_N + \underline{\underline{K}}_c\right)\end{aligned} \tag{2.105}$$

$$\underline{\underline{S}}_{12} = \underline{\underline{S}}_{21}^T = 2\left(\underline{\underline{E}}_N + \underline{\underline{K}}_c\right)\underline{\underline{D}}^T \left[\underline{\underline{D}}\left(\underline{\underline{E}}_N + \underline{\underline{K}}_c\right)\underline{\underline{D}}^T + 2\,\underline{\underline{E}}_n\right]^{-1} \tag{2.106}$$

$$\underline{\underline{S}}_{22} = \underline{\underline{S}}_{22}^T = \left[\underline{\underline{D}}\left(\underline{\underline{E}}_N + \underline{\underline{K}}_c\right)\underline{\underline{D}}^T + 2\,\underline{\underline{E}}_n\right]^{-1} \left[\underline{\underline{D}}\left(\underline{\underline{E}}_N + \underline{\underline{K}}_c\right)\underline{\underline{D}}^T - 2\,\underline{\underline{E}}_n\right] \quad (2.107)$$

2.6.5 Line terminations

Active and passive terminations are characterized by their multidimensional impedance and e.m.f. sources. The sources can be described by the equivalent Thevenin dipole representation:

$$\underline{V} = \underline{\mathcal{E}} - \underline{\underline{Z}}_G \underline{I} \quad (2.108)$$

where $\underline{\underline{Z}}_G$ is a diagonal matrix of the source impedances and $\underline{\mathcal{E}}$ is a column vector giving the e.m.f. of the sources. An equivalent representation for the waves in the reference basis $(\underline{\underline{U}}_R, \underline{\underline{J}}_R)$ writes:

$$\underline{A} = \underline{G} - \underline{\underline{K}}_G \underline{B} \quad (2.109)$$

where

$$\underline{\underline{K}}_G = \left(\underline{\underline{z}}_G + \underline{\underline{E}}_N\right)^{-1}\left(\underline{\underline{z}}_G - \underline{\underline{E}}_N\right) \quad (2.110)$$

$$\underline{G} = \left(\underline{\underline{z}}_G + \underline{\underline{E}}_N\right)^{-1}\underline{\underline{U}}_R \underline{\mathcal{E}} = \frac{1}{2}\left(\underline{\underline{E}}_N - \underline{\underline{K}}_G\right)\underline{\underline{U}}_R \underline{\mathcal{E}} \quad (2.111)$$

and $\underline{\underline{z}}_G = \underline{\underline{J}}_R^T \underline{\underline{Z}}_G \underline{\underline{J}}_R$ can be seen as a reduced source impedance.

Similarly, a passive load at the end of the line will be described by:

$$\underline{V} = \underline{\underline{Z}}_L \underline{I} \quad (2.112)$$

The relation between the corresponding waves is given by a reflection matrix $\underline{\underline{K}}_L$:

$$\underline{B} = \underline{\underline{K}}_L \underline{A} \quad (2.113)$$

where

$$\underline{\underline{K}}_L = \left(\underline{\underline{z}}_L + \underline{\underline{E}}_N\right)^{-1}\left(\underline{\underline{z}}_L - \underline{\underline{E}}_N\right) = \left(\underline{\underline{z}}_L - \underline{\underline{E}}_N\right)\left(\underline{\underline{z}}_L + \underline{\underline{E}}_N\right)^{-1} \quad (2.114)$$

and $\underline{\underline{z}}_L = \underline{\underline{J}}_R^T \underline{\underline{Z}}_L \underline{\underline{J}}_R$ is again a reduced impedance matrix.

2.6.6 Network analysis

A generic multidimensional network analysis tool has been developed, that is able to handle an arbitrary network topology, with any type of cable in the different network segments. The eigenmodes associated with each type of cable present in the network are first computed, as well as their fundamental parameters (eigenbase $(\underline{\underline{U}}_0, \underline{\underline{J}}_0)$, propagation factors $\{\gamma_n\}$). Simple reference bases $(\underline{\underline{U}}_R, \underline{\underline{J}}_R)$ are defined for each number of conductors. The multidimensional scattering matrices associated with each cable segment are then generated and converted in the appropriate reference basis. Using the scattering matrix algebra developed in the previous sections, and considering the exact nature of the various derivation and termination points, K transfer matrices $\underline{\underline{T}}_k$ are finally obtained, that relate the incoming wave vector on the k-th NT $\underline{A}_k$ to the source $\underline{G}$ generated at the LT :

$$\underline{A}_k = \underline{\underline{T}}_k \, \underline{G}. \tag{2.115}$$

The size of each transfer matrix actually depends on the number of conductors at the LT and at the different NTs. The network analysis is performed sequentially for all frequencies in the useful frequency range from 1 to 10 MHz.

2.7 Multipath channel model

The global network analysis method proposed in the previous section is extremely powerful as it is able to predict the channel responses associated with very elaborate networks including various types of cables with any number of conductors, any type of interconnection at the derivation points, and any type of termination load. In particular, the problem of mode mixture can be put forward : signals produced at the transmitter on a given eigenmode can be transferred to the other eigenmodes at some points of the network (unbalanced derivations or terminations). However, the physical interpretation of the obtained end-to-end channel frequency responses $H_k(\omega)$ is not straightforward. The channel impulse responses $h_k(\omega)$ can only be obtained by application of the inverse Fourier transform, which is also rather restrictive.

In order to obtain a better intuition about the end-to-end channel responses and the respective effects due to cable losses, derivations and terminations, we propose to set up a simple multipath model.

Four fundamental assumptions are necessary to validate this simple model :

1. Cables with *identical eigenmodes* are used throughout the network. The derivation and termination points are perfectly balanced, which ensures that the different modes do not mix to each other. In this scenario, the multiconductor network analysis can be reduced to the parallel analysis of independent scalar-waves networks.

2. *Derivation points* act independently of the frequency : the 3×3 scattering matrices associated with each eigenmode do not vary with frequency. This assumption is valid if the ratio of the respective characteristic impedances remains constant in the useful frequency range. It is also valid, of course, if the derivation cables are identical to the distribution cable.

3. *Termination points* also act independently of the frequency : they are modeled by a simple reflection coefficient in the whole frequency range and for each eigenmode. Ideal matched or open terminations satisfy this hypothesis.

4. Finally, the *propagation parameters* $\alpha_i(f)$ *and* $v_i(f)$ associated with a given eigenmode are the same for all cable segments. With this assumption, the channel response corresponding to a given path through the network only depends on the total path distance, irrespectively of the specific cable segments that belong to the considered path.

The multipath model expresses the end-to-end channel frequency response from the LT to the k^{th} NT as the sum :

$$H_k^{(i)}(\omega) = \sum_{l=1}^{N_p} a_{lk}^{(i)} \, e^{-\gamma_i(\omega)\, L_{lk}} \tag{2.116}$$

where

- $\left\{ a_{lk}^{(i)}, L_{lk} \right\}$ with $l \in [1, N_p]$ are the path weights and lengths. They only depend on the reflection and transmission coefficients related to the derivation and termination points. A given weight $a_{lk}^{(i)}$ generally results from the superposition of many distinct physical paths from the source to the destination, but all with the same total distance L_{lk}. The total number of paths N_p depends on the desired accuracy of the model. Mathematically, there is an infinite number of paths, but practically the number of significant paths is finite. The determination of N_p is a key parameter of the proposed multipath model.

- $\gamma_i(\omega) = f(\kappa, \delta_d, \delta_{c1}^{(i)})$ only depends on the propagation characteristics of the cables.

The resulting end-to-end channel impulse responses can be obtained as

$$h_k^{(i)}(t) = \sum_{l=1}^{N_p} a_{lk}^{(i)} \, h_{cd}^{(i)}(t, L_{lk}) \tag{2.117}$$

where the impulse response associated with a cable segment of length L_{lk} has been established in Section 2.4.

The computation of the path weights $\{a_{lk}\}$ and lengths $\{L_{lk}\}$ requires the analysis of a complex network including three types of elements ·

1. Two-acces ports representing the cable segments of length d_k or d'_k (see Figure 2.11). We assume that all cable segments have a length that is an integer multiple of a fundamental length L_0, i.e. $d_k = n_k L_0$ and $d'_k = n'_k L_0$ where n_k and n'_k are positive integers. In the example presented in Section 2.5, $L_0 = 5$ meter. The scattering matrix associated with a cable segment of length d_k is then given by

$$\underline{\underline{S}}_c(D) = \begin{pmatrix} 0 & D^{n_k} \\ D^{n_k} & 0 \end{pmatrix} \tag{2.118}$$

   where the symbolic variable D represents the propagation through a basic cable segment of length L_0.

2. Three-access ports representing the derivation points. Balanced and lossless derivations result in a scattering matrix given by

$$\underline{\underline{S}}_d = \begin{pmatrix} r_c & t_c & t_d \\ t_c & r_c & t_d \\ t_d & t_d & r_d \end{pmatrix} \tag{2.119}$$

   with $r_d^2 + 2t_d^2 = 1$ and $r_c^2 + t_c^2 + t_d^2 = 1$. The parameters r_c and r_d represent the reflection coefficients on the side of the distribution cable and on the side of the derivation cable, respectively. t_c gives the transmission coefficient along the distribution cable, and t_d gives the derivation coefficient. These parameters depend on the relative characteristic impedances of the cables. Let $\rho_{Z_c} = Z_{c2}/Z_{c1}$ be the ratio of the derivation cable impedance (Z_{c2}) and the distribution cable impedance (Z_{c1}). The different reflection and transmission coefficients in (2.119) are then given by

$$r_c = \frac{-1}{2\rho_{Z_c}+1} \qquad r_d = -\left(\frac{2\rho_{Z_c}-1}{2\rho_{Z_c}+1}\right) \tag{2.120}$$

$$t_c = \frac{2\rho_{Z_c}}{2\rho_{Z_c}+1} \qquad t_d = \frac{2\sqrt{\rho_{Z_c}}}{2\rho_{Z_c}+1} \tag{2.121}$$

In the special case where identical cables are used for the distribution and the derivation ($\rho_{Z_c} = 1$), these coefficients are $t_c = t_d = \frac{2}{3}$ and $r_c = r_d = -\frac{1}{3}$. This means that, on each derivation point, $\frac{1}{9}$ of the incoming energy is reflected, $\frac{4}{9}$ is derived and $\frac{4}{9}$ is transmitted along the distribution cable. A better transmission along the distribution cable (higher t_c, lower t_d, $|r_d|$ and $|r_c|$) is ensured for $\rho_{Z_c} > 1$.

3. Terminations that can be represented by a single reflection coefficient r_t.

The complex network is obtained by the interconnection of the elements depicted in the above list. By solving the network equations, the end-to-end transfer functions $T_k(D)$ can be obtained explicitly. They accept a Taylor expansion as follows :

$$T_k(D) = \sum_{j=0}^{\infty} \alpha_{jk}\, D^j \approx \sum_{l=1}^{N_p} a_{lk}\, D^{\frac{L_{lk}}{L_0}}. \tag{2.122}$$

The path weights $\{a_{lk}\}$ can be obtained by identification with the N_p first non-zero terms of the Taylor expansion.

Let us now analyze the network corresponding to the example given in Figure 2.12. All cable segments have a length that is an integer multiple of $L_0 = 5$ meter. The first path weight and length are given by (see also Table 2.2)

$$a_{1k} = t_c^{k-1}\, t_d \qquad L_{1k} = \sum_{j=0}^{k-1} d_j + d'_k. \tag{2.123}$$

For the type of cables used here ($\rho_{Z_c} = 1.8$, see Table 2.1), the transmission and derivation coefficients are $t_c = 0.78$ and $t_d = 0.58$ for the differential mode. Two successive paths are separated by a length of $2L_0 = 10$ meter. Figure 2.17 gives the normalized path weights obtained when all terminations are matched ($r_t(k) = 0 \quad \forall\ k$). The normalization is done with respect to the first path weight a_{1k}. In this scenario, the multipath effect can be exclusively attributed to the reflections on the derivation points. For example, the direct path from the LT to user 15 is 225 meter long and its weight is $a_{1,15} = t_c^{14} t_d = 0.019$. The second path is 235 meter long and corresponds to successive reflections on derivations $\{2,1\}$ and $\{11,10\}$. The corresponding weight is $a_{2,15} = 2r_c^2 a_{1,15} = 0.09 a_{1,15}$. The third path is 245 meter long and corresponds to successive reflections on derivations $\{2,1,2,1\}$, $\{2,1,11,10\}$, $\{11,10,11,10\}$, $\{5,4\}$, $\{6,5\}$ and $\{12,11\}$. The corresponding weight is then $a_{3,15} = (3r_c^2 + 3r_c^4) a_{1,15} = 0.15 a_{1,15}$. The next paths can be generated in the same way. Obviously, the relative weight of secondary paths increases with the user position k along the distribution cable.

For a unit energy wideband pulse transmitted at the LT, the received energy at each network termination is given by

$$\mathcal{E}_k^2 = \sum_{l=1}^{N_p} a_{lk}^2 \ < 1. \tag{2.124}$$

Considering both ends of the distribution cable as users 0 and $K+1$, the global power budget gives $\sum_{l=0}^{K+1} \mathcal{E}_k^2 = 1$. The set of parameters $\left\{\mathcal{E}_k^2\right\}$ reflects the distribution of the transmitted energy from the network head-end towards the different users. The first part of Figure 2.18 gives the distribution of $\mathcal{E}_k^2$ in dB vs. the user index k for different values of the transmission factor t_c. The energy loss increases dramatically with the user position, especially for low values of t_c. The straight lines give the contribution of the first path weight, as given by (2.123). As expected, the relative strength of the secondary paths increases with k and with t_c (as can be observed by the divergence of the curves). The circles give the total received energy for a transmitted passband pulse in the range of 1 MHz to 10 MHz. The second part of Figure 2.18 gives the evolution of the received energy vs. the transmission factor t_c in the range of $\frac{2}{3}$ to 0.95, for users 2, 5, 10, 15 and 20. It can be observed that the inequality of the energy distribution can be moderated by increasing the transmission coefficient t_c. For lower values of t_c, the existence of the secondary paths also moderates the effect of energy dilution for remote users, but this gain is lost as soon as the passband pulse is taken into account in the power budget.

The observation made here is a crucial feature of the powerline access networks : the total energy transmitted by the LT is delivered in very unequal parts to the various users. The PLC network was not initially designed to

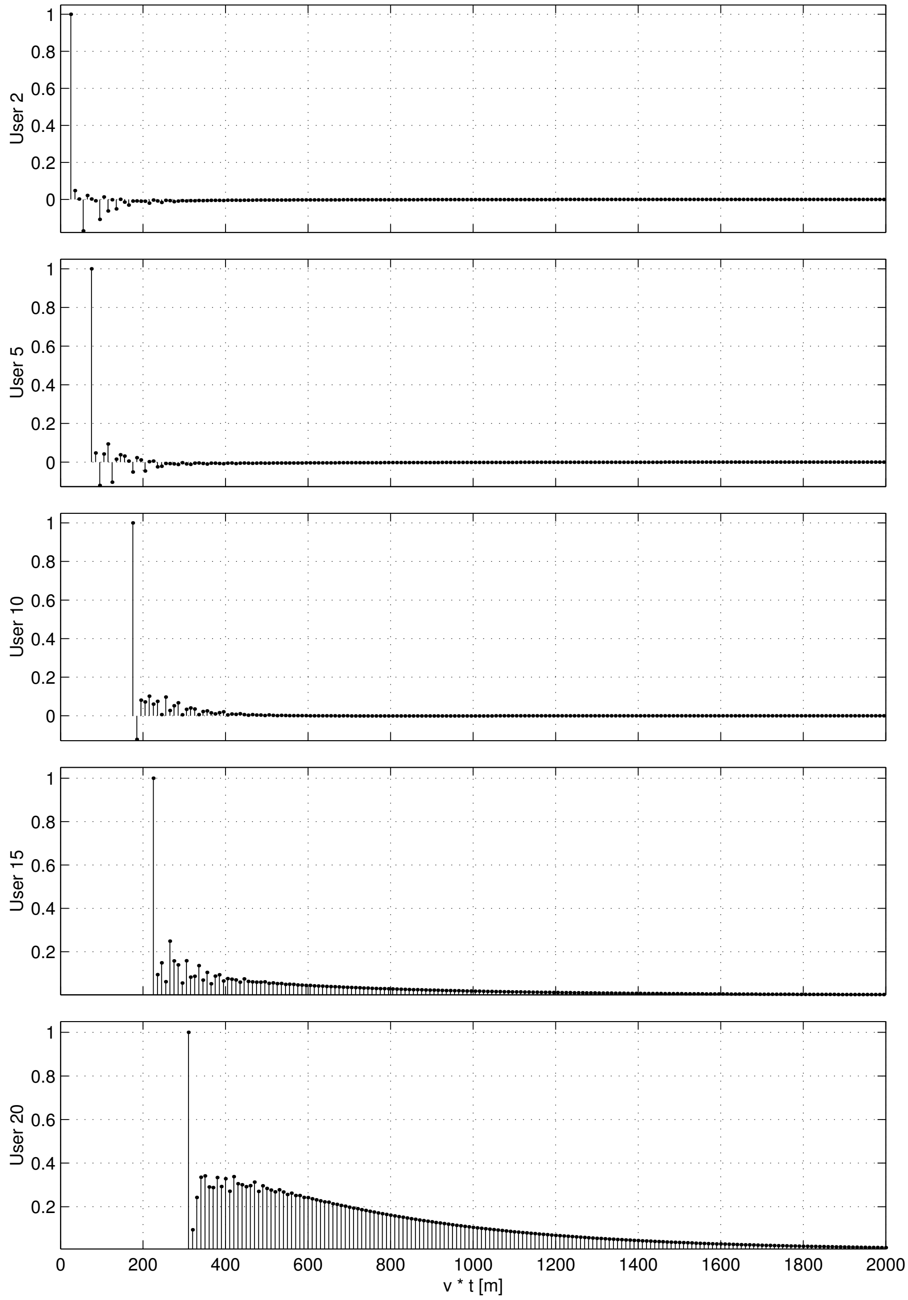

Figure 2.17: *Weights with matched terminations (normalized w.r.t. the first path weight)*

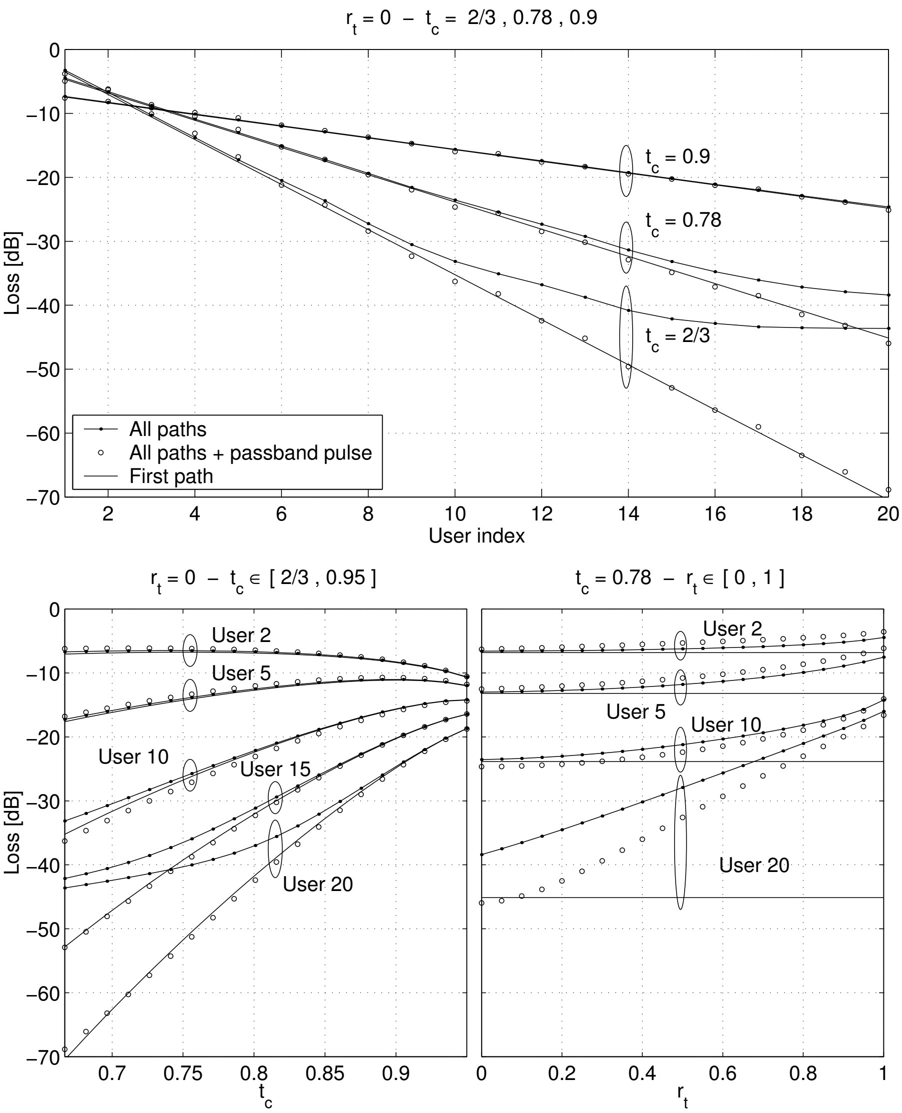

Figure 2.18: *Influence of network parameters on the total energy distributed to the different users : t_c (transmission factor along the main cable) and r_t (reflection factor at unused terminations)*

convey high-frequency signals to the subscribers. At very low frequency (e.g. the power frequency), what really matters is the sum of the path weights, which can be shown to be

$$H_k(f \approx 0) = \sum_{l=1}^{N_p} a_{lk} = \frac{2}{K+2} \quad \forall\, k \in (1, \cdots, K) \tag{2.125}$$

for identical loads at all network terminations. A balanced power distribution network can thus become very unbalanced at high frequency.

Figure 2.19 gives the normalized path weights obtained when all unused terminations are left open ($r_t(k) = 1 \quad \forall\ k \notin \{2, 5, 10, 15, 20\}$). In that scenario, a high number of additional physical paths have to be taken into account as the waves are also reflected on the open terminations. The relative importance of the secondary paths is considerably increased, especially for the remote users : for some of them, the first path is not even the strongest one any more. The energy distribution is less unbalanced than in the previous scenario : one reason for this is that the total energy delivered by the LT is now dissipated in 5 termination loads instead of $K + 1$ as before. The last part of Figure 2.18 gives the evolution of the received energy vs. the reflection factor r_t at unused terminations in the range of 0 (matched) to 1 (open), for users 2, 5, 10 and 20.

2.8 PLC channel responses

This section is devoted to the derivation of the final end-to-end channel responses $H_k(\omega) = \mathcal{F}\{h_k(t)\}$ associated with the network example of Figure 2.12.

The channel impulse responses $h_k(t)$ actually result from the combined effect of :

- The multiple paths from the LT to the NTs through the multiple reflections on cable derivations and network terminations. The path weight distribution was analyzed in Section 2.7 in relation with the *network topology*.

- The *conductor and dielectric losses*, which increase with the distance. The impulse response associated with a cable segment was presented in Section 2.4.

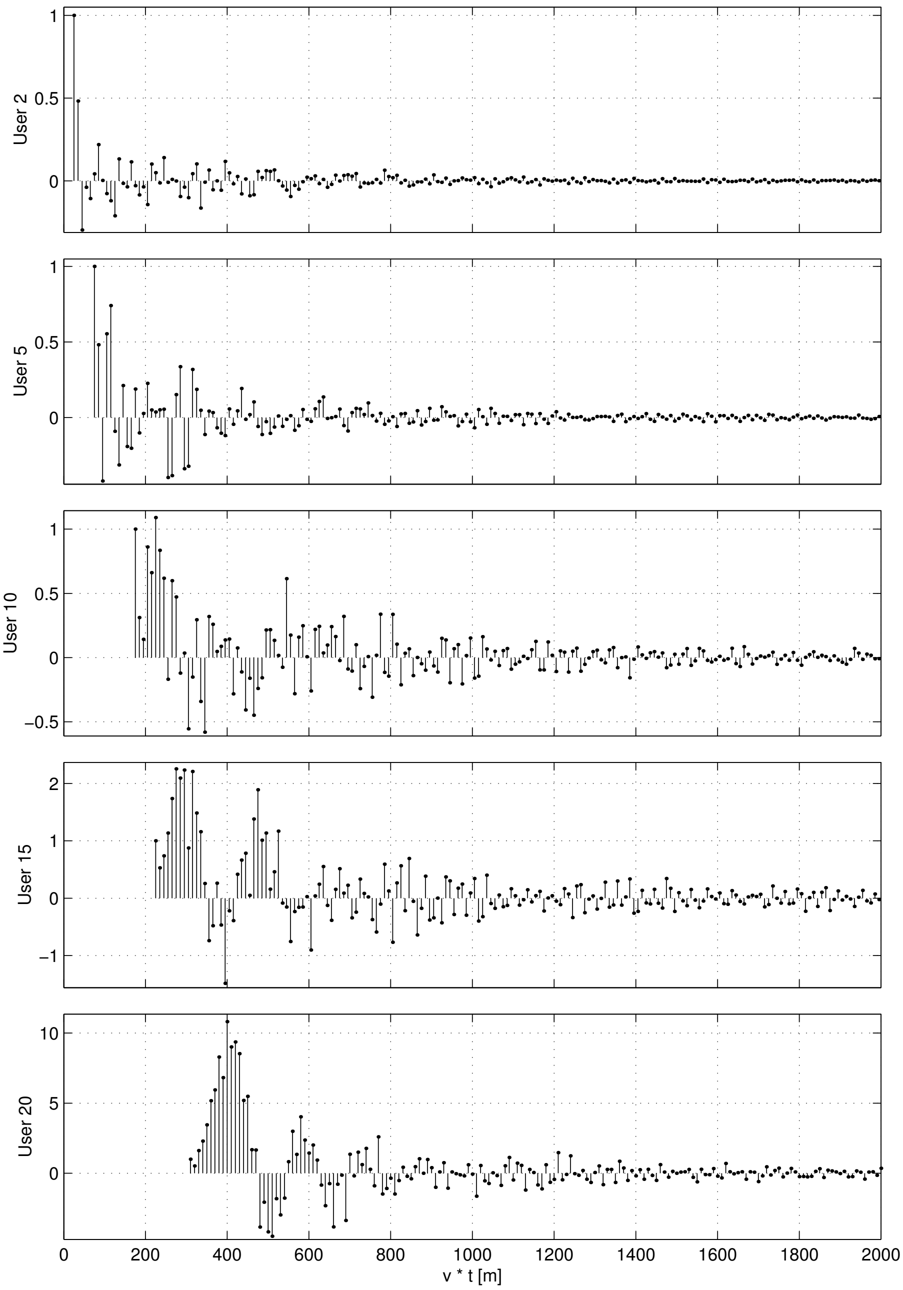

Figure 2.19: *Weights with open terminations (normalized w.r.t. the first path weight)*

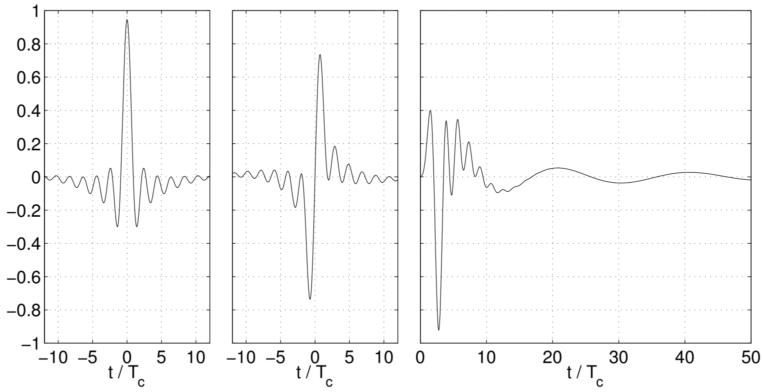

Figure 2.20: *Passband pulses : cosine modulated half-root Nyquist pulse (left, $\alpha = 0.15$), sine modulated half-root Nyquist pulse (middle, $\alpha = 0.15$) and analog filters impulse response (right)*

- The analog front end of the modems. One of their functions is to restrict the spectrum of the transmitted signals to the frequency band authorized for the high-speed PLC application, i.e. 1 MHz to 10 MHz. It is equivalent to consider the transmission of a passband pulse. Figure 2.20 gives three types of passband pulses (with $0.5/T_c =$ 10 MHz).

Figure 2.21 illustrates the combination of the path weights (vertical segments) with a baseband half-root Nyquist pulse, for users 2 and 20. The delay difference between two successive paths is here approximately 50 ns (for 10 meter difference and a phase velocity close to 2.10^8 m/s), which corresponds to the baseband pulse period : $T_c = 50$ ns. For the network topology chosen here, the successive paths are then only just resolvable. The bold curves include the additional effect of cable losses. The number of significant paths is then decreased as longer paths are more affected by the cable attenuation.
Figure 2.22 gives the final impulse responses $h_k(t)$ for users 2, 5, 10, 15 and 20, with a passband pulse. The thin curves include a cosine-modulated half-root Nyquist pulse while the bold curves include analog bandpass filters (elliptic filters). The passband pulses are illustrated in Figure 2.20.

Finally, the amplitude of the end-to-end channel frequency responses $|H_k(\omega)|^2$ (in dB) is given in Figure 2.23, in the frequency range of 0 to 25 MHz :

- The upper figure displays the 20 channel responses obtained with

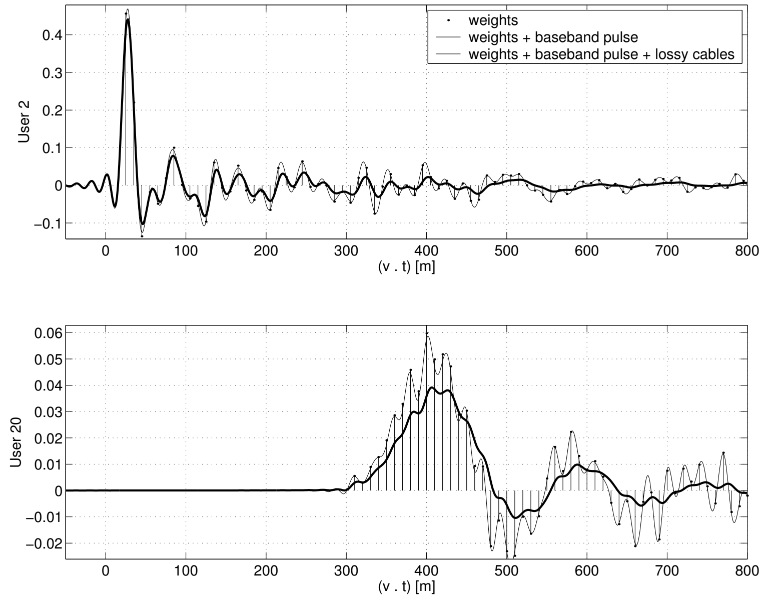

Figure 2.21: *Combination of path weights and a baseband pulse*

all-matched terminations, using the multipath model proposed in (2.116). Only the differential propagation mode is represented. The vertical ordering of the curves is in accordance with the channel index k : the higher curve corresponds to $H_1(\omega)$, the lower one corresponds to $H_{20}(\omega)$. Bold curves are used to highlight channels 2, 5, 10, 15 and 20. For these channels, the exact channel responses, as obtained by the scattering matrix formalism, are also given (dashed lines). Obviously, the multipath approximation is extremely accurate.

- The lower figure displays the 5 channel responses obtained when the unused terminations are left open. The scattering matrix formalism was used to derive exact channel responses. Here, the 3 modes of propagation (differential, phantom and common) are represented and can be compared.

2.9 Conclusion

It has been demonstrated that the channel transfer functions corresponding to practical outdoor PLC networks could be modeled analytically with the

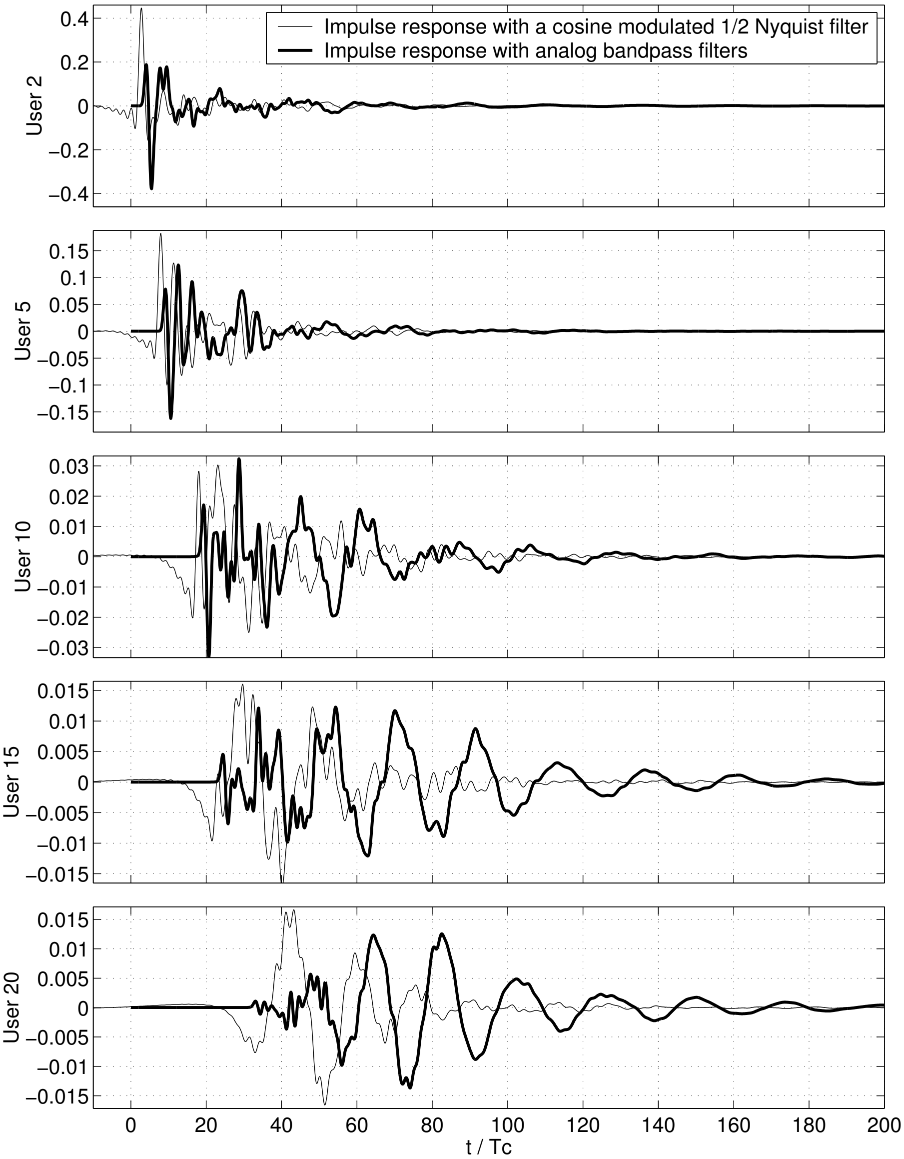

Figure 2.22: *Final impulse responses with open terminations (differential mode)*

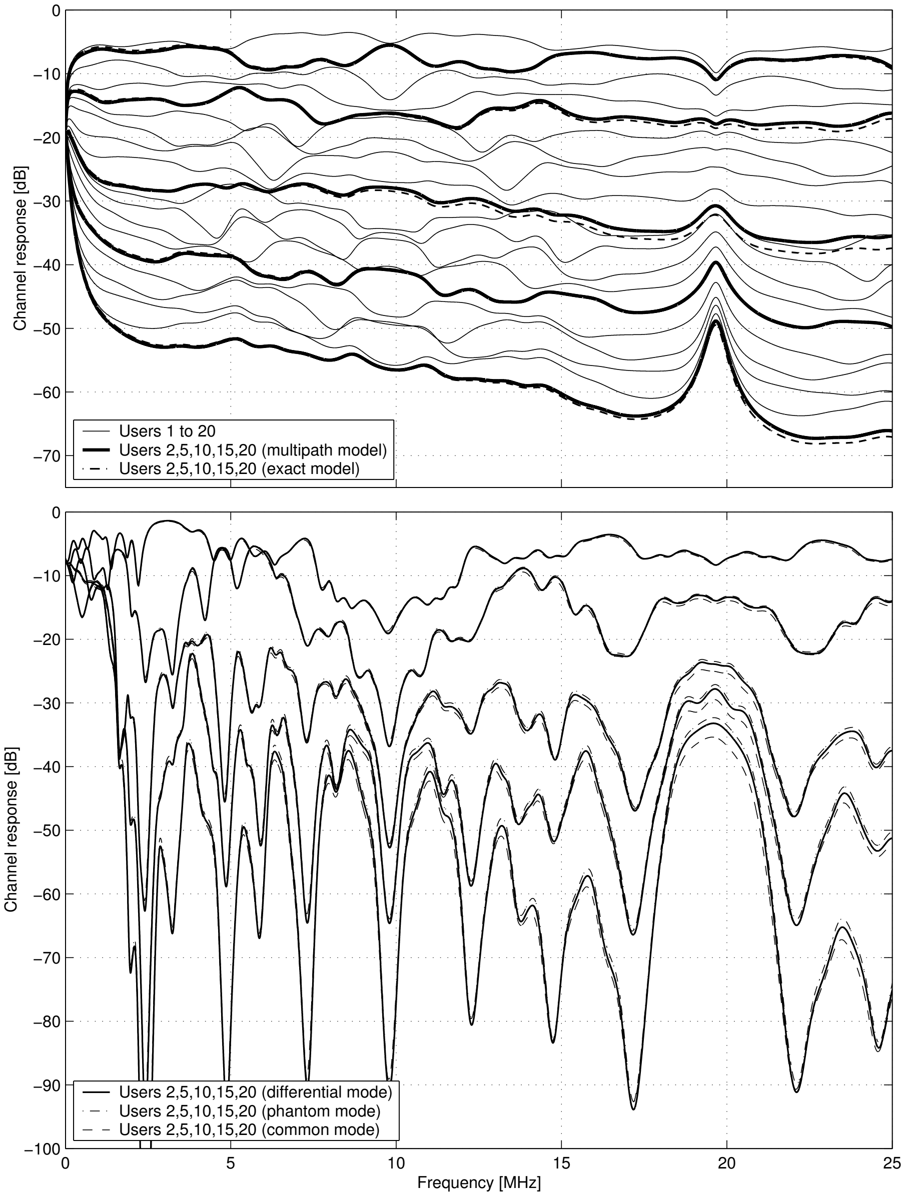

Figure 2.23: *Frequency responses with matched terminations (up) and open terminations (down)*

help of the multiconductor transmission line theory. The complete analysis combines two steps : the analysis of the multiconductor cables, and the analysis of the full network topology.

In the first step, the fundamental characteristics of the different types of multiconductor cables are derived. This analysis requires the resolution of an eigenvalue problem for each cable type, which leads to the definition of propagation eigenmodes, i.e. specific distributions of voltages and currents in the different conductors, that propagate with a unique propagation factor (including phase velocity and specific attenuation), and that are characterized by a well-defined characteristic impedance. Practical PLC cables have been analyzed, and the propagation eigenmodes (differential mode, common mode, phantom mode) have been derived as a function of the cable geometry and the used materials (conductors and dielectrics). A characteristic impedance of a few ohms (common mode) up to a few tens of ohms (differential mode) was found. The conductor losses (skin effect) were shown to be dependent on the propagation mode, due to the proximity effect. However, the difference was found to be rather small from one mode to another. The fundamental impulse response corresponding to the propagation over a given cable segment of a given length was analyzed in details. Three specific contributions were put forward : a propagation delay, an impulse due to conductor losses, and an impulse due to dielectric losses.

The second step combines the various cable segments (characterized by a given length and a given set of propagation modes with their own parameters) with the network discontinuities: derivations (cable interconnections) and terminations. Progressive and regressive multi-dimensional waves (one wave for each eigenmode) propagate along each cable segment. Multi-dimensional transmission and reflection happen on each network transition. This can be modeled accurately with the help of multi-dimensional scattering matrices.

The end-to-end channel transfer functions in the range of 1 to 50 MHz were derived for a practical PLC network including a main cable of 300 m, 20 derivations, and three types of 4-conductor cables. The channel responses associated with each eigenmode were found to be very close to each other. In the selected example, the 4 different propagations modes are well separated, which corresponds to 4 parallel and independent channels. In a more complex scenario, however, the different eigenmodes could be combined, depending on the cable interconnections and the diversity of the cables used in the network.

The channel losses were found to increase dramatically with the position of the user along the main cable. The fundamental reason for this is not the increased distance with respect to the cable headend, but rather the high number of derivations along the main cable, with important power losses at each derivation. The respective impacts of open and matched terminations were also compared.

Finally, the end-to-end channel impulse responses were derived. They were found to be a combination of a multipath channel (with a distribution of weights and distances that depends on the network topology and cable impedances) and the impulse responses resulting from conductor and dielectric losses. Between 50 and 100 significant paths were found for the selected example.

The PLC channel frequency responses derived in this Chapter will be used in Chapter 3 to obtain the capacity region of the powerline channel.